First-principles calculations of structural, electronic, vibrational, and magnetic properties of C-60 and C48N12

Xie, R. H.; Bryant, G. W.; Jensen, L.; Smith, V. H.

Published in:
Journal of Chemical Physics

DOI:
10.1063/1.1566742

Publication date:
2003

First-principles calculations of structural, electronic, vibrational, and magnetic properties of C_{60} and $C_{48}N_{12}$: A comparative study

Rui-Hua Xie, Garnett W. Bryant, Lasse Jensen, Jijun Zhao, and Vedene H. Smith

Citation: J. Chem. Phys. **118**, 8621 (2003); doi: 10.1063/1.1566742
View online: https://doi.org/10.1063/1.1566742
View Table of Contents: http://aip.scitation.org/toc/jcp/118/19
Published by the American Institute of Physics

First-principles calculations of structural, electronic, vibrational, and magnetic properties of C_{60} and $C_{48}N_{12}$: A comparative study

Rui-Hua Xie[a] and Garnett W. Bryant
Atomic Physics Division, National Institute of Standards and Technology, Gaithersburg, Maryland 20899-8423

Lasse Jensen
Materials Science Centre, Rijksuniversiteit Groningen, Nijenborgh 4, 9747 AG Groningen, The Netherlands

Jijun Zhao
Department of Physics and Astronomy, University of North Carolina at Chapel Hill, Chapel Hill, North Carolina 27599

Vedene H. Smith, Jr.
Department of Chemistry, Queen's University, Kingston, ON K7L 3N6, Canada

(Received 9 December 2002; accepted 19 February 2003)

The structural, electronic, vibrational, and magnetic properties of the $C_{48}N_{12}$ azafullerene and C_{60} are comparatively studied from the first-principles calculations. Full geometrical optimization and Mulliken charge analysis are performed. Electronic structure calculations of $C_{48}N_{12}$ show that the highest occupied molecular orbital (HOMO) is a doubly degenerate level of a_g symmetry and the lowest unoccupied molecular orbital (LUMO) is a nondegenerate level of a_u symmetry. The calculated binding energy per atom and HOMO-LUMO energy gap of $C_{48}N_{12}$ are about 1 eV smaller than those of C_{60}. Because of electron correlations, the HOMO-LUMO gap decreases about 5 eV and the binding energy per atom increases about 2 eV. The average second-order hyperpolarizability of $C_{48}N_{12}$ is about 55% larger than that of C_{60}. Our vibrational frequency analysis predicts that $C_{48}N_{12}$ has 58 infrared-active and 58 Raman-active vibrational modes. Two different methods for calculating nuclear magnetic shielding tensors of C_{60} and $C_{48}N_{12}$ are compared, and we find that $C_{48}N_{12}$ exhibits eight ^{13}C and two ^{15}N NMR spectral signals. Our best-calculated results for C_{60} are in excellent agreement with experiment. Our results suggest that $C_{48}N_{12}$ has potential applications as semiconductor components, nonlinear optical materials, and possible building blocks for molecular electronics and photonic devices. © *2003 American Institute of Physics.* [DOI: 10.1063/1.1566742]

I. INTRODUCTION

The macroscopic synthesis[1] of soot, which contains C_{60} and other fullerenes in large compounds, plus the straightforward purification techniques which make the pure fullerene materials available, have led to extensive studies of fullerenes.[2–5] Doped fullerenes have also attracted a great deal of interest due to their remarkable structural, electronic, optical, and magnetic properties.[2–5] The unique structural and electronic properties of fullerenes[2] led to another type of doping, named *substitutional doping*,[2–5] where one or more carbon atoms of fullerene are substituted by other atoms, as well as the endohedral doping and exohedral doping. Because boron and nitrogen bracket carbon in the Periodic Table, much attention has been paid to alternate boron- and/or nitrogen-doped compounds.[2–5] Over the past 10 years, boron and nitrogen atoms have been successfully used to replace carbon atoms of C_{60} and synthesize many kinds of heterofullerenes, $C_{60-m-n}N_mB_n$.[2–9] Very recently, the existence of a novel $C_{48}N_{12}$ aza-fullerene[9–11] has been reported. Hence, it would be interesting and useful to investigate and predict the structural, electronic, vibrational and magnetic properties of this aza-fullerene by performing detailed first-principles calculations. This forms the main purpose of the present paper.

Fullerenes have been challenging molecules for first-principles calculations because of their size.[12,13] Recent advances in *ab initio* methods and parallel computing have brought a substantial improvement in capabilities for predicting the properties of large molecules. The coupled cluster method has been used to predict phenomena in C_{20}.[14] Other first-principles methods, which are less demanding in terms of computation cost than the coupled cluster method, have been used for much larger fullerenes and carbon nanotubes. For example, C_{60} (Refs. 15–20) has been studied with self-consistent field (SCF) and Møller–Plesset second-order (MP2) theory, C_{240} (Ref. 21) with density functional theory (DFT),[22] and C_{540} (Ref. 23) with the Hartree–Fock (HF) method.

In Sec. II, we perform full geometry optimizations of $C_{48}N_{12}$ as well as C_{60} with both DFT and restricted HF (RHF) methods. It is found that the $C_{48}N_{12}$ aza-fullerene has

[a]Electronic mail: rhxie@nist.gov

several distinguishing features: only one nitrogen atom per pentagon, two nitrogen atoms preferentially sitting in one hexagon, S_6 symmetry, six unique nitrogen–carbon (NC), and nine unique CC bonds. The Mulliken charge analysis shows that the nitrogen atoms in $C_{48}N_{12}$ exist as electron acceptors and three-fourths of the carbon atoms as electron donors. Our best CC bond lengths and radius of C_{60} calculated with B3LYP/6-31G* are in excellent agreement with experiment.

Total energy calculations of the optimized $C_{48}N_{12}$ and C_{60} are discussed in Sec. III. For both molecules, the total energies calculated with STO-3G and 6-31G basis sets differ from the 6-31G* results by about 1.5% and 0.05%, respectively, and the HOMO-LUMO gaps decrease about 5 eV due to electron correlations. For C_{60}, our calculated results are in agreement with other groups' calculations, and our best HOMO-LUMO energy gap calculated with B3LYP/6-31G* agrees well with experiment.

When an external electric field is applied to a molecule, its charges are redistributed and dipoles are induced or reoriented.[3] The relation between the dipole moment $\mathbf{P}$ and the applied field $\mathbf{G}$ can be written as $\mathbf{P}=\mathbf{P}_0+\alpha\mathbf{G}+(\beta/2)\mathbf{G}^2+\gamma/6\mathbf{G}^3+\cdots$,[3] where $\mathbf{G}$ is the electric field, $\mathbf{P}_0$ is the permanent dipole moment, α is the dipole polarizability, β is the first-order hyperpolarizability, and γ is the second-order hyperpolarizability. The static dipole polarizability (SDP) measures the ability of the valence electrons to find a configuration which screens a static external field,[3] while the hyperpolarizability plays a key role in the description of nonlinear optical phenomena of a material.[3] In Sec. IV, we calculate the SDPs and second-order hyperpolarizabilities of $C_{48}N_{12}$ and C_{60}. The calculated SDP for C_{60} is in agreement with experiment. The average second-order hyperpolarizability of $C_{48}N_{12}$ is about 55% larger than that of C_{60}.

When a material is doped, its mechanical, electronic, magnetic and optical properties would change.[2–5] The ability to control such induced changes is vital to progress in material science. Raman and infrared (IR) spectroscopic techniques[24] are useful experimental tools to investigate how doping modifies the structural and dynamical properties of the pristine material and to understand the physical origin of such induced changes. Over the past 10 years, both techniques have been used widely to study the vibrational properties of C_{60}.[25,26] It has been shown that C_{60} has in total 46 vibrational modes including 4 IR-active[25,26] and 10 Raman-active vibrational modes.[26] These studies have offered a good guide to the phonon spectrum in the solid state of these materials. In Sec. V, we perform a vibrational analysis and calculate the infrared (IR) intensities of $C_{48}N_{12}$. Twenty nine doubly-degenerate and 29 nondegenerate IR-active, and 29 doubly-degenerate unpolarized and 29 nondegenerate polarized Raman-active frequencies are determined. The best vibrational frequencies and IR results for C_{60} calculated with B3LYP are in excellent agreement with experiment. Comparison with other groups' calculations of C_{60} is made and discussed.

High resolution NMR (Ref. 27) gives spectra which can be analyzed to yield parameters such as the nuclear magnetic shielding σ,[28] which characterizes molecular systems and structures and is determined by the electronic environments of the nuclei involved. In Sec. VI, the gauge-including atomic orbital (GIAO) and the continuous set of gauge transformations (CSGT) methods[29] are utilized for calculating the nuclear magnetic shielding tensor σ in $C_{48}N_{12}$ and C_{60} at both the HF and DFT levels of theory. Eight ^{13}C and two ^{15}N NMR spectral signals are predicted for $C_{48}N_{12}$. Our best calculated NMR results for C_{60} are in excellent agreement with experiment.

Finally, we end in Sec. VII by giving a summary and outlook on the potential applications of $C_{48}N_{12}$.

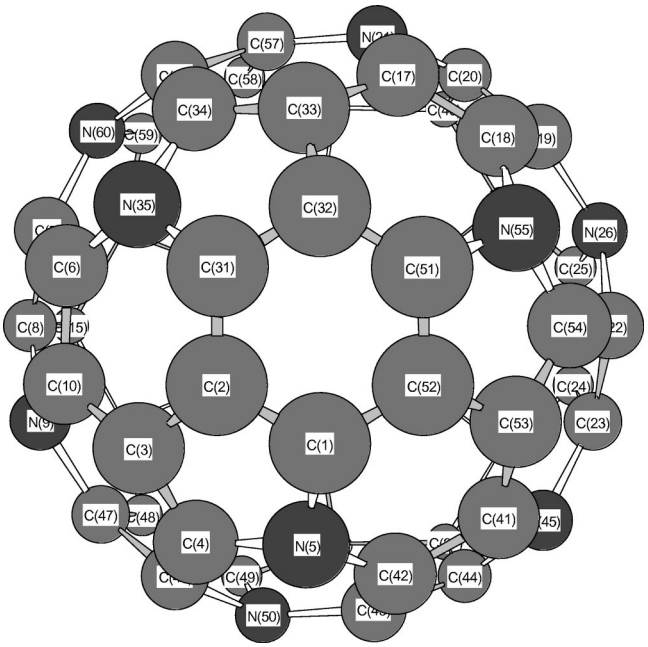

FIG. 1. Geometric structure of $C_{48}N_{12}$ azafullerene. The site numbers {5, 9, 14, 21, 26, 30, 35, 39, 45, 50, 55, 60} are for nitrogen atoms, while the others are for carbon atoms.

II. OPTIMIZED GEOMETRIC STRUCTURE

The geometries of both $C_{48}N_{12}$ and C_{60} were fully optimized by using the GAUSSIAN 98 program,[30,31] where we have employed both RHF and DFT methods. Also we discuss the effects of basis sets. For the DFT method, we use the B3LYP hybrid functional.[32]

In Fig. 1, we present the geometry of $C_{48}N_{12}$. The *ab initio* calculations show that $C_{48}N_{12}$ has only one nitrogen atom per pentagon and two nitrogen atoms preferentially sit in one hexagon. The symmetry of $C_{48}N_{12}$ is the S_6 point group.[10,11] The optimized distances (or radii) R_i from the ith atom to the density center of the molecule are listed in Table I. We find that there are 10 unique radii for $C_{48}N_{12}$, which suggest that $C_{48}N_{12}$ is an ellipsoidal structure and has 10 unique sites (2 for N sites and 8 for C sites), while C_{60} has an equal radius for each carbon atom. As shown in Sec. VI, the 10 unique sites of $C_{48}N_{12}$ can be identified by NMR experiments. For the same basis set, comparing the B3LYP results with the RHF results shows that the radii are increased by up to 2% due to the electron correlation. Comparing the 6-31G and 6-31G*'s results shows that adding polarization func-

TABLE I. Net Mulliken charge Q_i ($q=1.6\times10^{-19}$) and radius R_i (1 Å = 0.1 nm) at the site number n_i in $C_{48}N_{12}$ and C_{60} calculated by the B3LYP method with a variety of Pople-style basis sets and RHF method with 6-31G*.

			B3LYP/STO-3G		B3LYP/6-31G		B3LYP/6-31G*		RHF/6-31G*	
Fullerene	Site number $\{n_i\}$	Atom	R_i (Å)	Q_i/q (C)	R_i (Å)	Q_i/q (C)	R_i (Å)	Q_i/q (C)	R_i (Å)	Q_i/q (C)
$C_{48}N_{12}$	{1, 13, 16, 31, 38, 51}	C	3.5871	0.0827	3.5365	0.2147	3.5171	0.1961	3.4988	0.2926
	{2, 12, 29, 32, 37, 52}	C	3.5923	−0.0188	3.5458	−0.0175	3.5275	−0.0125	3.5162	−0.0621
	{3, 11, 28, 33, 36, 53}	C	3.6019	−0.0193	3.5492	−0.0173	3.5395	−0.0298	3.5389	−0.0480
	{4, 15, 27, 34, 40, 54}	C	3.5951	0.0682	3.5408	0.2486	3.5190	0.2266	3.4716	0.3167
	{5, 14, 30, 35, 39, 55}	N	3.7175	−0.1883	3.5945	−0.6690	3.6187	−0.5953	3.6151	−0.7803
	{6, 18, 24, 42, 48, 58}	C	3.5092	0.0550	3.4706	0.1985	3.4348	0.1919	3.3880	0.2209
	{7, 19, 23, 43, 47, 57}	C	3.4882	0.0679	3.4465	0.2103	3.4049	0.2124	3.3409	0.2962
	{8, 20, 22, 44, 46, 56}	C	3.5431	0.0618	3.4946	0.2623	3.4720	0.1998	3.4416	0.2433
	{9, 21, 26, 45, 50, 60}	N	3.6302	−0.1814	3.5304	−0.7047	3.5335	−0.6002	3.5082	−0.7829
	{10, 17, 25, 41, 49, 59}	C	3.5554	0.0723	3.5087	0.2548	3.4807	0.2110	3.4222	0.3036
C_{60}	{1, 2, 3, 4, 5, 6, ..., 60}	C	3.6034	0	3.5615	0	3.5502	0	3.5226	0

tions decreases the radius of carbon sites but increases the radius of nitrogen sites. In comparison with the results of STO-3G and 6-31G basis sets, we find that increasing the basis size would lead to a decreased radius. For C_{60}, the radius for each carbon site calculated by using B3LYP and the 6-31G* basis set is 3.5502 Å, which is in excellent agreement with experiment ($R=3.55$ Å),[33] the local density approximation (LDA) calculation ($R=3.537$ Å) with a pseudopotential approach (PPA),[34] and the LDA-based Car–Parrinello molecular dynamics (CPMD) simulation ($R=3.55$ Å).[35]

The calculated net Mulliken charges Q_i of carbon and nitrogen atoms in $C_{48}N_{12}$ are also listed in Table I. There are two unique types of nitrogen atoms in the structure. The net Mulliken charges Q_i/q ($q=1.6\times10^{-19}$) on both types of N are negative, for example, −0.5953 C and −0.6002 C with B3LYP/6-31G*, −0.7803 C and −0.7829 C with RHF/6-31G*. The net Mulliken charges of the carbon atoms in $C_{48}N_{12}$ separate into two groups: 1/4 of carbon atoms with negative Q_i and the remaining 3/4 with positive Q_i. Although the Mulliken charge analysis cannot estimate the atomic charges quantitatively, their signs can be estimated.[36] From these results, we find that the nitrogen atoms and one-fourth of the carbon atoms exist as electron acceptors, and three-fourths of the carbon atoms as electron donors. It should be mentioned that we also performed calculations of net Mulliken charges of carbon and boron atoms in $C_{48}B_{12}$.[37] We found that the boron atoms exist as electron donors and all carbon atoms as electron acceptors.[37] Therefore, $C_{48}N_{12}$ and $C_{48}B_{12}$ have opposite electronic polarizations, while C_{60} is isotropic. With respect to the electron correlation and the choice of basis sets, we find that the absolute value of the net Mulliken charge Q_i for each atom in $C_{48}N_{12}$ increases with an increase of the basis size, but decreases due to the electron correlation or by adding polarization functions to a given basis set.

The optimized CC and NC bond lengths in $C_{48}N_{12}$ are listed in Table II. We find that there are 6 unique NC and 9 unique CC bonds. In comparison with the calculated CC bond lengths for C_{60} shown in Table II, the CC bond length in $C_{48}N_{12}$, in general, is less than the single C–C bond length of C_{60} due to the redistribution of the electron density. It is also found that the bond length increases due to the electron correlation, but decreases as we increase the basis size or include the polarization function.

In comparison with experimental data available for C_{60} listed in Table III, we find that the two kinds of bond lengths of C_{60} calculated by using the B3LYP with a large basis set 6-31G* are in good agreement with the results measured by x-ray powder diffraction (XRPD),[38] NMR,[39,40] gas-phase electron diffraction (GPED) (Ref. 41) or x-ray crystallography technique (XRCT).[33]

For comparison, Table III also lists the calculated CC bond lengths for C_{60} with a selection of previous theoretical calculations. Given the low computational cost of Hückel theory, the bond lengths[42] predicted by this theory are remarkably satisfactory. The semiempirical QCFF/PI (quantum-chemical-force-fields for π electrons) (Ref. 43) does not predict as good bond lengths as the Hückel theory since it has been parameterized mainly with respect to frequencies of conjugated hydrocarbons. The CC bond lengths calculated by using the semiempirical modified neglect of differential overlap (MNDO) (Ref. 44) and the extended Hubbard model (EHM) (Ref. 45) are a little improved. These theoretical approaches empirically include the effect of electron correlation found in conjugated π-systems. The HF (Refs. 15–17, 20) and self-consistent field with MO (SCFMO) (Ref. 19) calculations are in agreement with our RHF results. As listed in Table III, the calculated MP2 bond distances[18] usually decrease by about 0.01 Å when more d functions are added to the basis set, demonstrating the necessity of including polarization functions in calculations with correlation. Based on the differences between the HF and MP2 data, it is evident that electron correlation effects should be considered in an accurate description of the equilibrium structure of a molecule. The CC bond lengths calculated with the LDA,[46–48] LDA-PPA,[34] and LDA-based CPMD simulation[35,49] are in agreement with our B3LYP's results.

As mentioned before, C_{60} has only two kinds of bond angles,[2] 108° (the angle between two adjacent single C–C

TABLE II. Bond lengths (L, 1 Å = 0.1 nm) in $C_{48}N_{12}$ and C_{60} calculated by using B3LYP methods with a variety of Pople-style basis sets, where (n_i, n_j) denotes the site number pair that forms a bond.

			STO-3G		3-21G		6-31G		6-31G*	
Fullerene	Bond	(n_i, n_j)	L_{dft} (Å)	L_{rhf} (Å)	L_{dft} (Å)	L_{rhf} (Å)	L_{dft} (Å)	L_{rhf} (Å)	L_{dft} (Å)	L_{rhf} (Å)
$C_{48}N_{12}$	CC	(1, 2) (12, 13) (16, 29) (31, 32) (37, 38) (51, 52)	1.4275	1.3914	1.4103	1.3855	1.4125	1.3880	1.4061	1.3836
	CC	(1, 52) (2, 31) (12, 38) (13, 29) (16, 37) (32, 51)	1.4371	1.4151	1.4171	1.4083	1.4216	1.4134	1.4155	1.4024
	NC	(1, 5) (13, 14) (16, 30) (31, 35) (38, 39) (51, 55)	1.4742	1.4601	1.432	1.4206	1.4315	1.4164	1.4300	1.4272
	CC	(2, 3) (11, 12) (28, 29) (32, 33) (36, 37) (52, 53)	1.4701	1.4662	1.4517	1.4524	1.4488	1.4478	1.4455	1.4521
	CC	(3, 4) (11, 15) (27, 28) (33, 34) (36, 40) (53, 54)	1.4092	1.3590	1.3947	1.3620	1.3971	1.3652	1.3901	1.3588
	CC	(3, 10) (11, 59) (17, 33) (25, 36) (28, 49) (41, 53)	1.4559	1.4566	1.4320	1.4350	1.4346	1.4367	1.4314	1.4368
	NC	(4, 5) (14, 15) (27, 30) (39, 40) (34, 35) (54, 55)	1.4707	1.4553	1.4307	1.4128	1.4286	1.4108	1.4224	1.4047
	CC	(4, 46) (8, 15) (20, 40) (22, 54) (27, 44) (34, 56)	1.4567	1.4589	1.4326	1.4367	1.4354	1.4388	1.4313	1.4372
	NC	(5, 42) (6, 35) (14, 48) (18, 55) (24, 30) (39, 58)	1.4749	1.4637	1.4299	1.4294	1.4317	1.4278	1.4287	1.4310
	CC	(6, 7) (18, 19) (23, 24) (42, 43) (47, 48) (57, 58)	1.4399	1.4352	1.4211	1.4182	1.4217	1.4185	1.4136	1.4143
	CC	(6, 10) (17, 18) (24, 25) (58, 59) (41, 42) (48, 49)	1.4119	1.3641	1.3963	1.3664	1.4004	1.3712	1.3941	1.3634
	CC	(7, 8) (19, 20) (22, 23) (43, 44) (46, 47) (56, 57)	1.4195	1.3705	1.4021	1.3718	1.4068	1.3761	1.4021	1.3703
	NC	(7, 60) (9, 47) (19, 26) (21, 57) (23, 45) (43, 50)	1.4586	1.4419	1.4159	1.4047	1.4189	1.4071	1.4099	1.3958
	NC	(8, 9) (20, 21) (22, 26) (44, 45) (46, 50) (56, 60)	1.4510	1.4313	1.4182	1.4083	1.4149	1.4012	1.4084	1.4056
	NC	(9, 10) (17, 21) (25, 26) (41, 45) (49, 50) (59, 60)	1.4612	1.4360	1.4271	1.4043	1.4226	1.3997	1.4134	1.3919
C_{60}	C═C	(1, 52) (2, 31) (3, 10)···	1.4130	1.3759	1.3899	1.3671	1.3981	1.3750	1.3949	1.3732
	C–C	(1, 2) (1, 5) (2, 3)···	1.4773	1.4628	1.4601	1.4529	1.4592	1.4524	1.4539	1.4487

bonds) and 120° (the angle between a double C═C bond and an adjacent single C–C bond). We calculate the distribution of (C–C–C, C–N–C, C–C–N) bond angles in $C_{48}N_{12}$ calculated by using both RHF and B3LYP methods with several different basis sets. We found that one-third and two-thirds of the bond angles in $C_{48}N_{12}$ fluctuate around 108° and 120°, respectively. Especially, we noticed that the effect of electron correlation or increasing the basis size (for example, from STO-3G to 6-31G) leads to smaller fluctuations in the bond angle distribution (BAD) around either 108° or 120°, while enhanced fluctuations in the BAD are observed as polarization functions are added to the 6-31G basis set [see Figs. 2(a) and 2(b)].

III. TOTAL ELECTRONIC ENERGY

We performed total energy calculations of $C_{48}N_{12}$ and C_{60} by using both RHF and B3LYP with STO-3G, 6-31G, and 6-31G* basis sets. The results are summarized in Table IV. The orbital energies are shown in Fig. 3, where the orbital symmetries are also labeled.

Table IV demonstrates the convergence of the total energy calculations of both RHF and B3LYP methods with respect to the basis sets. For both $C_{48}N_{12}$ and C_{60}, the total energies calculated with STO-3G and 6-31G basis sets differ from the 6-31G* basis set results by about 1.5% and 0.05%, respectively. Our RHF results agree with the SCF results calculated by Scuseria *et al.*[15–17,20] For both molecules, comparing the B3LYP and RHF results shows that the HOMO-LUMO energy gap Δ decreases about 5 eV and the binding energy E_b per atom increases about 2 eV because of the electron correlations. The calculated binding energy E_b per atom and HOMO-LUMO energy gap Δ of $C_{48}N_{12}$ are about 1 eV smaller than those of C_{60}.

Because of the valency of the doped nitrogen atoms, the electronic properties of $C_{48}N_{12}$ and C_{60} are significantly different. As shown in Figs. 3(a) and 3(b), the HOMO for C_{60} is fivefold-degenerate with h_u symmetry, the LUMO is threefold-degenerate with t_{1u} symmetry, and the others are threefold-degenerate with t_{1g} or t_{2u} symmetry, fourfold-degenerate with g_g or g_u symmetry, and fivefold-degenerate with h_g symmetry. We notice from Fig. 3 that each energy level in $C_{48}N_{12}$ splits since the icosahedral symmetry of C_{60} is lost by the substitutional doping. For $C_{48}N_{12}$, the HOMO is a doubly degenerate level of a_g symmetry, the LUMO is a nondegenerate level with a_u symmetry, and the others are specified in Fig. 3. Considering that $C_{48}N_{12}$ is isoelectronic with C_{60}^{-12}, we find that the filling of the energy levels in

TABLE III. Equilibrium CC bond lengths (1 Å = 0.1 nm) of C_{60} from previous theoretical predictions and experimental findings. STO-DZP and DNP denote double-zeta STO's and double numerical basis with polarization functions, respectively.

Method	C–C (Å)	C=C (Å)	Reference
Hückel	1.436	1.418	42
QCFF/PI	1.471	1.411	43
MNDO	1.465	1.376	44
EHM	1.446	1.402	45
SCFMO	1.49	1.43	19
HF/STO-3G	1.463	1.376	15
HF/3-21G	1.453	1.367	20
HF/DZ	1.451	1.368	16
HF/STO-3G	1.463	1.376	17
HF/DZ	1.451	1.368	17
HF/DZP	1.450	1.375	17
HF/TZP	1.448	1.370	17
MP2/DZ	1.470	1.407	18
MP2/DZP	1.451	1.412	18
MP2/TZP	1.446	1.406	18
LDA/STO-DZP	1.436	1.384	48
LDA/DZP	1.445	1.395	47
LDA/DNP	1.444	1.391	46
LDA-PPA	1.449	1.390	34
LDA-CPMD	1.45	1.40	35
LDA-CPMD	1.45	1.39	49
Exp./XRCT	1.4459	1.3997	33
Exp./XRPD	1.455	1.391	38
Exp./NMR	1.45	1.40	39
Exp./NMR	1.46	1.40	40
Exp./GPED	1.458	1.401	41

$C_{48}N_{12}$ corresponds to a complete filling of the t_{1u} and t_{1g} levels of C_{60}.

In Table IV, we list the calculated ionization potential (IP) E_{IP} and electron affinity (EA) E_{EA} for both C_{60} and $C_{48}N_{12}$. It shows that $C_{48}N_{12}$ is a good electron donor, while C_{60} is a good electron acceptor. The calculated IP for C_{60} is in good agreement with the experiments: (7.54 $\pm$0.01) eV,[50] (7.57$\pm$0.01) eV,[51] ($7.58^{+0.04}_{-0.02}$) eV,[52] and (7.59$\pm$0.02) eV.[53] The calculated EA for C_{60} agrees well with the experiments: (2.666$\pm$0.001) eV,[54] (2.689 $\pm$0.008) eV.[55]

In crystals, the on-site Coulomb interaction[56] between two electrons on the same molecule is given by $U = U_{\mathrm{free}} - 2\mathrm{E}_p$, where $U_{\mathrm{free}} = \mathrm{E_{IP}} - \mathrm{E_{EA}} - \Delta$ is the on-site Coulomb interaction between two electrons on the free molecule[2] and $\mathrm{E}_p = z\alpha e^2/(2L^4)$ (z, the number of nearest neighbors; L, the distance between molecules, α, the dipole polarizability) is the polarization energy. Our plane-wave pseudopotential calculations performed by using the CASTEP program[31,57] show that the optimized lattice constants for C_{60} and $C_{48}N_{12}$-based fcc solids (note: $z=12$ for both cases) are all around 1.45 nm, while the experimental lattice constant=1.4161 nm for C_{60}.[58] Based on our first principles results for E_{IP}, E_{EA}, and Δ for C_{60} and $C_{48}N_{12}$ molecules, we arrive at the value of the on-site Coulomb interaction, U=1.84,2.05 eV for C_{60} and $C_{48}N_{12}$ solids, respectively. The experimental values for C_{60} are U=1.6$\pm$0.2 eV (Ref. 56) and 1.54 eV.[59] Moreover, our DFT/GGA calculations show that the band gap E_{gap} for the $C_{48}N_{12}$ solid is about 0.85 eV smaller than that of C_{60}. This

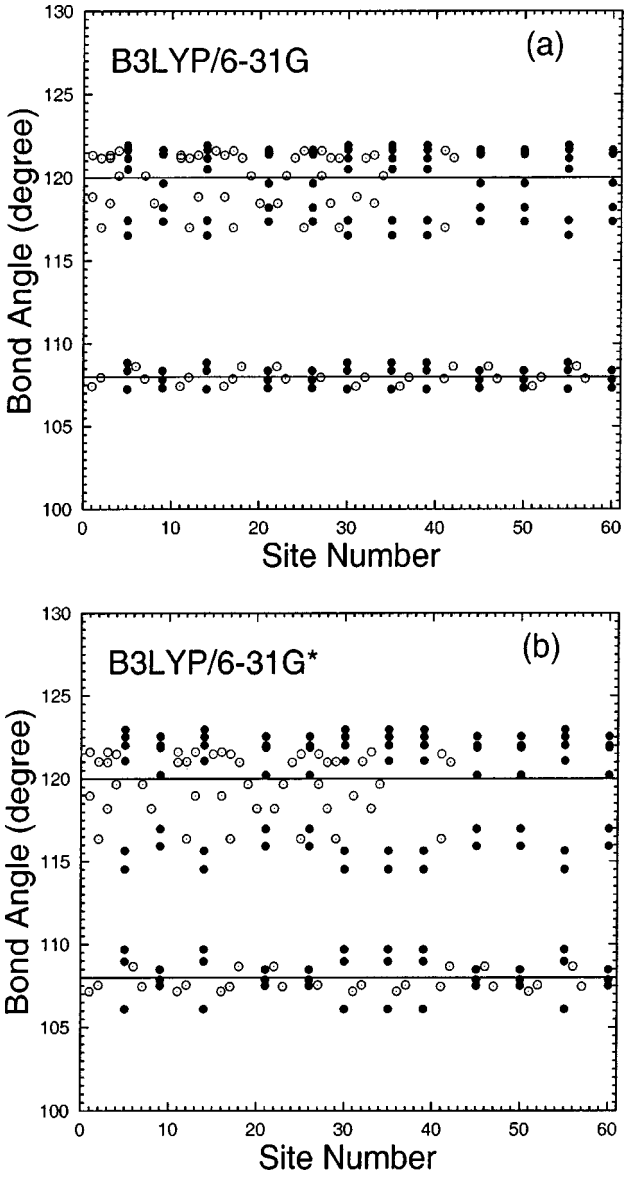

FIG. 2. *Ab initio* calculations of C–C–C (open circles) and C–N–C (or C–C–N) (filled circles) bond angles in $C_{48}N_{12}$: (a) B3LYP/6-31G and (b) B3LYP/6-31G*. The site numbers are labeled in Fig. 1. The solid lines are the C–C–C bond angles (108° and 120°) of C_{60}.

is consistent with the Δ-U-W relation,[2] $E_{\mathrm{gap}} = \Delta + U - W$, where W is the bandwidth for the HOMO- or LUMO-derived energy bands. Assuming the same W for both $C_{48}N_{12}$ and C_{60} solids, we arrive at $E_{\mathrm{gap}}^{\mathrm{C_{48}N_{12}}} \approx E_{\mathrm{gap}}^{\mathrm{C_{60}}} - 0.79$ eV.

The DFT is known to underestimate the band gap of solids. From experiment, $E_{\mathrm{gap}} = 2.3 \pm 0.1$ eV (Ref. 56) and 2.86 eV (Ref. 59) for the C_{60} solid. Hence, using the approximate relation given above, we obtain an estimated band gap for the $C_{48}N_{12}$ fcc solid of $E_{\mathrm{gap}}^{\mathrm{C_{48}N_{12}}} = 1.7 \pm 0.3$ eV. Thus, the $C_{48}N_{12}$ solid, like C_{60}, is a semiconducting material. Similarly, we find that the $C_{48}B_{12}$-based fcc solid (lattice constant $\approx$1.45 nm) is also a semiconducting material,[37] having $U = 1.9$ eV, $E_{\mathrm{gap}}^{\mathrm{C_{48}B_{12}}} - E_{\mathrm{gap}}^{\mathrm{C_{60}}} = -1.34$ eV, and $E_{\mathrm{gap}}^{\mathrm{C_{48}B_{12}}} = 1.2 \pm 0.3$ eV.

TABLE IV. Total electronic energy (E_t, in eV), LUMO energy (E_{lumo}, in eV), HOMO energy (E_{homo}, in eV), HOMO-LUMO energy gap (Δ, in eV), binding energy per atom (E_b, in eV), ionization potential (E_{IP}, in eV) and electron affinity (E_{EA}, in eV) of $C_{48}N_{12}$ and C_{60} calculated by using RHF and B3LYP methods with a variety of Pople-style basis sets.

		C_{60}			$C_{48}N_{12}$		
Method	Energy	STO-3G	6-31G	6-31G*	STO-3G	6-31G	6-31G*
RHF	E_t	−61 067.132	−61 795.062	−61 817.394	−66 397.387	−67 193.956	−67 223.547
	E_{lumo}	2.688	−0.709	−0.117	3.797	0.214	0.643
	E_{homo}	−5.456	−7.919	−7.644	−3.287	−6.203	−6.189
	Δ	8.144	7.210	7.527	7.084	6.417	6.832
	E_b	5.581	4.666	4.956	4.510	3.724	4.149
	E_{IP}	4.892	5.685	5.659	2.45	5.314	5.530
	E_{EA}	2.280	1.187	1.125	1.947	0.209	0.267
B3LYP	E_t	−61 446.662	−62 194.006	−62 209.002	−66 795.835	−67 617.031	−67 637.724
	E_{lumo}	−1.127	−3.390	−3.219	−0.188	−2.706	−2.614
	E_{homo}	−4.356	−6.221	−5.987	−2.365	−4.633	−4.383
	Δ	3.229	2.831	2.768	2.177	1.927	1.774
	E_b	7.715	6.843	6.982	6.888	6.088	6.365
	E_{IP}	3.868	8.576	7.317	2.488	5.600	5.663
	E_{EA}	1.487	1.073	2.398	0.804	0.223	1.493

IV. STATIC (HYPER)POLARIZABILITY

The static polarizabilities for $C_{48}N_{12}$ and C_{60} are presented in Table V. The B3LYP and RHF results are obtained by using the GAUSSIAN 98 program package[30,31] and the LDA results by using the Amsterdam Density Functional (ADF) program.[31,60,61] The ADF program uses basis sets of Slater functions, where a triple zeta valence basis plus polarization is augmented with the field-induced polarization (FIP) functions of Zeiss *et al.*[62] Here this basis set is denoted as TZP $++$ ($[6s4p2d1f]$ for C and N atoms) and has recently been used for calculating the second-order hyperpolarizabilities, γ, for C_{60}, $C_{58}N_2$, $C_{58}B_2$, and $C_{58}BN$.[63]

From the results listed in Table V, we see that the basis set dependence is identical for both B3LYP and RHF cases. As expected, improving the basis set increases the polarizability. Our RHF results for C_{60} are in good agreement with a previous study[64] which used a similar method and basis sets. The B3LYP values are about 10% larger than the corresponding RHF values. The LDA results are much larger than both the B3LYP and RHF results. This is expected since the basis set is larger and expected to predict a more accurate polarizability.[63] Also LDA, in general, predicts a larger polarizability than does with B3LYP.[65] The LDA results for C_{60} are in good agreement with previous LDA studies.[66–68] We find that the polarizability of $C_{48}N_{12}$ is slightly smaller than the polarizability of C_{60}. For $C_{48}N_{12}$ we also find that the zz component is slightly larger than the xx component except when using RHF.

Very recently, using the molecular beam deflection technique, Antoine *et al.*[69] have measured the electric polarizability of isolated C_{60} molecules and obtained a value of $(76.5\pm 8.0)\times 10^{-30}$ m^3. Using a new optical technique that uses light forces and a time-of-flight spectrometer, Ballard *et al.*[70] have made absolute measurements of cluster polarizabilities and determined the optical polarizability of C_{60} at the fundamental wavelength of a Nd:YAG laser ($\lambda = 1064$ nm) to be $(79\pm 4)\times 10^{-30}$ m^3. The experimental results are in good agreement with our LDA results, especially considering that LDA is expected to overestimate the polarizability.

The static second-order hyperpolarizabilities for $C_{48}N_{12}$ and C_{60} molecules are presented in Table VI. For the calculations of the second-order hyperpolarizability, γ, we use time-dependent (TD) DFT as described in Refs. 63, 67, 71, 72. First, the first-order hyperpolarizability, β, is calculated analytically in the presence of a small electric field. Then, the second-order hyperpolarizability can be obtained by a finite-field differentiation of the analytically calculated first-order hyperpolarizability. For all the TD-DFT calculations we used the RESPONSE code[31,71,73] implemented in the ADF program.[31,60,61] The small difference between γ_{xxzz} and γ_{zzxx} for $C_{48}N_{12}$ is due to the numerical method adopted for calculating γ.

For the γ value of C_{60}, we find good agreement with previous first-principles results.[3,4,67,68,74] A comparison with experiments will not be made for the second-order hyperpolarizability due to large differences in the experimental results.[3,4,67,74] We find that all components of the second-order hyperpolarizability for $C_{48}N_{12}$ are larger than for C_{60}. This gives an average second-order hyperpolarizability of $C_{48}N_{12}$ which is about 55% larger than the average second-order hyperpolarizability of C_{60}. The $zzzz$ components of the second-order hyperpolarizaility of $C_{48}N_{12}$ is also larger than that found in the donor/acceptor substituted $C_{58}BN$ molecule.[63]

V. VIBRATIONAL FREQUENCY ANALYSIS

A. Normal vibrations in C_{60} and $C_{48}N_{12}$

Using the GAUSSIAN 98 program,[30,31] we calculated the harmonic vibrational frequencies of both C_{60} and $C_{48}N_{12}$ and considered the effects of the basis sets. It should be mentioned that our frequencies have not been scaled.

Table VII and VIII summarize the vibrational frequen-

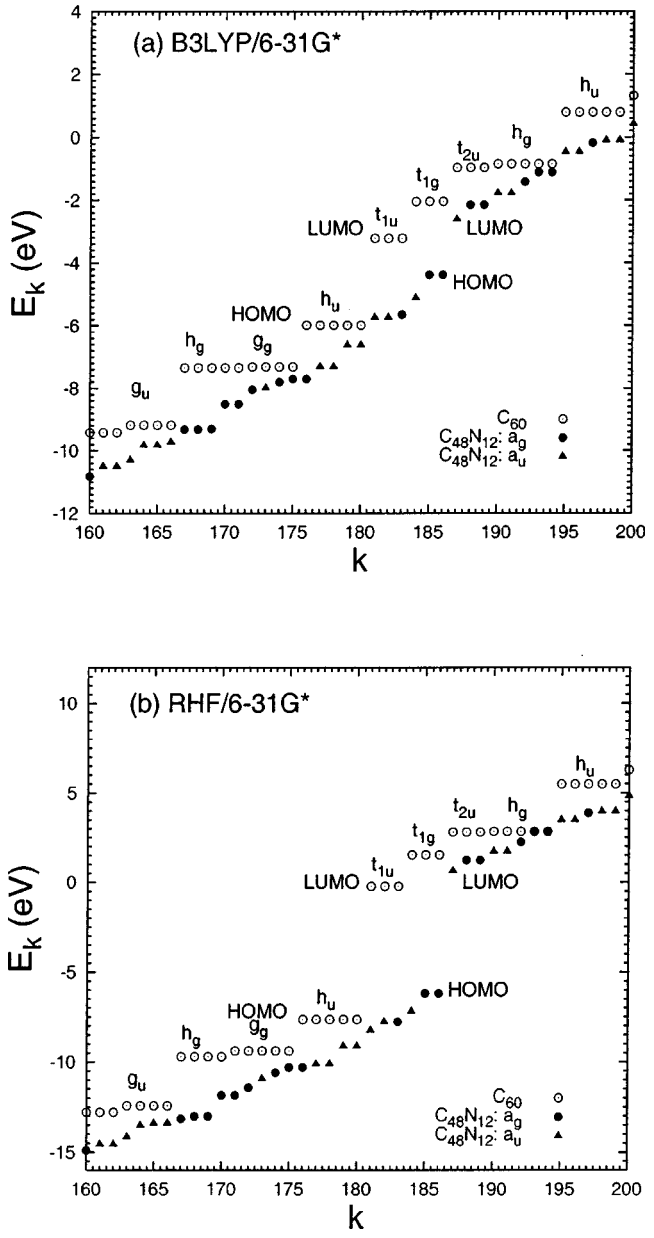

FIG. 3. Orbital energies E_k of the kth eigenstate of C_{60} (open circles) and $C_{48}N_{12}$ (filled circles and triangles) with (a) B3LYP/6-31G* and (b) RHF/6-31G*. The orbital symmetries of energy levels are shown.

cies for C_{60} calculated by using RHF and B3LYP methods, respectively. There are 46 vibrational modes for C_{60}, which are classified in even and odd parities and in ten irreducible representatives of the I_h point group: the $\{a_g, a_u\}$, $\{t_{1g}, t_{1u}, t_{2g}, t_{2u}\}$, $\{g_g, g_u\}$, and $\{h_g, h_u\}$ modes are non-, threefold-, fourfold- and fivefold-degenerate, respectively. Tables VII and VIII demonstrate that increasing the basis size improves the accuracy of the predicted vibrational frequencies, but adding polarization functions to the 6-31G basis set only improves slightly the accuracy of the vibrational frequencies. In choosing a basis set for the first-principles calculation, one must make a compromise between accuracy and CPU time. Our results shows that the minimum calculation can be done in about 4 h of CPU, while the most expensive calculation requires 12 days of CPU.

TABLE V. Static polarizabilities (α, in $Å^3 = 10^{-30}$ m^3) for $C_{48}N_{12}$ and C_{60} with RHF and DFT methods and a variety of basis sets. Symmetry relations give for C_{60}, $\alpha_{xx} = \alpha_{yy} = \alpha_{zz}$, and for $C_{48}N_{12}$, $\alpha_{xx} = \alpha_{yy}$.

	3-21G		6-31G		6-31G*		TZP++
	B3LYP	RHF	B3LYP	RHF	B3LYP	RHF	LDA
C_{60}							
α_{xx}	64.9	59.5	68.3	63.2	69.5	64.7	84.7
$C_{48}N_{12}$							
α_{xx}	62.0	55.6	65.6	59.4	66.6	60.0	79.3
α_{zz}	62.6	54.9	66.1	58.5	67.5	60.4	81.5

Without significant computational cost, one can do B3LYP/STO-3G calculation and still obtain results more accurate than any RHF calculations. Going beyond STO-3G for B3LYP calculations requires a drastic increase in CPU time. Surprisingly, going just to 3-21G provides the most accurate results, while for the bigger basis set 6-31G, the results are worse and adding a polarized function to 6-31G only slightly improves the results. The 3-21G basis set gives systematically lower frequencies than the 6-31G basis set, while the frequencies obtained from the 6-31G* basis set typically lie between the results of the other two basis sets. In contrast, as discussed in Sec. II, 6-31G* does provide the most accurate bond lengths. This suggests that the better accuracy of 3-21G is fortuitous. Increasing the basis set to 6-31G stiffens the bonds, while adding the polarization function compensates by softening the bonds. In comparison to the B3LYP results, RHF calculated frequencies are too high due to an incorrect description of bond dissociation, while B3LYP with large basis sets (even the minimum basis set STO-3G) generally gives results in good agreement with the experiments of Wang *et al.*[25] and Dong *et al.*[26] This demonstrates the importance of electron correlation in an accurate description of the vibrational frequencies.

For comparison, Table VII lists the vibrational frequencies of C_{60} calculated by using various theories, for example, the semiempirical MNDO (Ref. 44) and QCFF/PI (Ref. 43) methods. Of these, the QCFF/PI method, which has been parameterized mainly with respect to vibrational frequencies of conjugated and aromatic hydrocarbons,[75] results in the best results although it gives less satisfactory geometry. Such accurate prediction implies that the electronic structures of C_{60} is not much different from other aromatic hydrocarbons.[43] Häser *et al.*[18] showed that the approximate harmonic frequencies for the two a_g vibrational modes of C_{60} are 1615 cm^{-1} and 487 cm^{-1} for HF/DZP, 1614 cm^{-1} and 483 cm^{-1} for HF/TZP, 1614 cm^{-1} and 437 cm^{-1} for

TABLE VI. Static second-order hyperpolarizabilities (γ, in au., 1 a.u. $= 6.235\,378 \times 10^{-65}$ $C^4\,m^4\,J^{-3}$) for $C_{48}N_{12}$ and C_{60} calculated using LDA and TZP++. The average second-order hyperpolarizability is given by $\overline{\gamma} = \frac{1}{15}\Sigma_{i,j}(\gamma_{iijj} + \gamma_{ijij} + \gamma_{ijji})$. Symmetry relations give $\gamma_{xxxx} = \gamma_{yyyy}$, $\gamma_{xxzz} = \gamma_{yyzz}$, and $\gamma_{zzxx} = \gamma_{zzyy}$.

	γ_{xxxx}	γ_{xxyy}	γ_{zzzz}	γ_{xxzz}	γ_{zzxx}	$\overline{\gamma}$
C_{60}	137950	45983	137950	45983	45983	137950
$C_{48}N_{12}$	188780	62880	232970	85120	84790	215222

TABLE VII. Vibrational frequencies (ν, in cm^{-1}) of C_{60} calculated with RHF and a variety of Pople-style basis sets. Numbers in the parenthesis are the relative errors to the experimental frequencies, ν^{exp}, from Wang *et al.* (Ref. 25) and Dong *et al.* (Ref. 26). The approximated CPU times for STO-3G, 3-21G, 6-31G, and 6-31G* basis sets are 5 h, 12 h, 18 h, and 39 h, respectively. Results of other theoretical calculations, for example, QCFF/PI (Ref. 43), MNDO (Ref. 44), and MFCM (Ref. 79), are also listed.

Mode	STO-3G	3-21G	6-31G	6-31G*	QCFF/PI	MFCM	MNDO	Expt.
				Even parity				
a_g	1684 (14.5%)	1604 (9.1%)	1637 (11.3%)	1600 (8.9%)	1442 (1.9%)	1468 (0.1%)	1667 (13.4%)	1470
	553 (11.0%)	518 (4.0%)	526 (5.7%)	527 (5.7%)	513 (3.0%)	492 (1.2%)	610 (22.5%)	498
g_g	1802 (18.2%)	1667 (9.3%)	1697 (11.3%)	1687 (10.6%)	1585 (3.9%)	1521 (0.3%)	1650 (8.2%)	1525
	1531 (12.9%)	1426 (5.1%)	1450 (6.9%)	1441 (6.3%)	1450 (6.9%)	1375 (1.4%)	1404 (3.5%)	1356
	1203 (11.8%)	1095 (1.8%)	1142 (6.2%)	1132 (5.2%)	1158 (7.6%)	1056 (1.9%)	1235 (14.8%)	1076
	908 (12.6%)	787 (2.3%)	878 (9.0%)	836 (3.8%)	770 (4.5%)	805 (0.1%)	856 (6.2%)	806
	653 (5.2%)	646 (4.1%)	643 (3.5%)	619 (0.3%)	614 (1.1%)	626 (0.8%)	579 (6.9%)	621
	574 (18.0%)	529 (9.0%)	549 (12.9%)	537 (10.5%)	476 (2.1%)	498 (2.5%)	491 (1.0%)	486
h_g	1912 (21.2%)	1772 (12.3%)	1799 (14.0%)	1791 (13.5%)	1644 (4.2%)	1575 (0.2%)	1722 (9.1%)	1578
	1658 (16.2%)	1546 (8.4%)	1585 (11.1%)	1562 (9.4%)	1465 (2.7%)	1401 (1.8%)	1596 (11.8%)	1427
	1482 (18.4%)	1326 (6.0%)	1377 (10.1%)	1380 (10.3%)	1265 (1.1%)	1217 (2.7%)	1407 (12.5%)	1251
	1290 (17.2%)	1184 (7.5%)	1208 (9.8%)	1208 (9.7%)	1154 (4.8%)	1102 (0.1%)	1261 (14.5%)	1101
	886 (14.3%)	828 (6.9%)	843 (8.6%)	840 (8.4%)	801 (3.4%)	788 (1.7%)	924 (19.2%)	775
	836 (17.6%)	761 (7.1%)	821 (15.4%)	794 (11.7%)	691 (2.8%)	708 (0.4%)	771 (8.4%)	711
	509 (17.5%)	475 (9.7%)	496 (14.5%)	482 (11.4%)	440 (1.6%)	439 (1.4%)	447 (3.2%)	433
	302 (10.7%)	295 (8.0%)	296 (8.3%)	289 (5.9%)	258 (5.5%)	269 (1.5%)	263 (3.7%)	273
t_{1g}	1505 (10.9%)	1371 (0.9%)	1403 (3.3%)	1404 (3.4%)	1398 (2.9%)	1346 (0.9%)	1410 (3.8%)	1358
	966 (1.0%)	940 (3.7%)	939 (3.8%)	916 (6.1%)	975 (0.1%)	981 (0.5%)	865 (11.4%)	976
	687 (36.9%)	618 (23.1%)	670 (33.4%)	640 (27.5%)	597 (18.9%)	501 (0.2%)	627 (24.9%)	502
t_{2g}	1619 (19.1%)	1453 (6.9%)	1504 (10.6%)	1511 (11.1%)	1470 (8.1%)	1351 (0.7%)	1483 (9.0%)	1360
	912 (0.2%)	907 (0.8%)	898 (1.8%)	868 (5.0%)	890 (2.6%)	931 (1.8%)	919 (0.5%)	914
	903 (4.3%)	701 (19.0%)	828 (4.3%)	734 (15.1%)	834 (3.6%)	847 (2.1%)	784 (9.4%)	865
	647 (14.1%)	637 (12.3%)	634 (11.7%)	613 (8.1%)	637 (12.3%)	541 (4.6%)	591 (4.2%)	567
				Odd parity				
a_u	1111 (2.8%)	1112 (2.5%)	1097 (4.1%)	1061 (7.2%)	1206 (5.5%)	1142 (0.1%)	972 (15.0%)	1143
g_u	1701 (17.7%)	1562 (8.0%)	1607 (11.1%)	1597 (10.4%)	1546 (6.9%)	1413 (2.3%)	1587 (9.8%)	1446
	1527 (16.6%)	1406 (7.3%)	1447 (10.5%)	1437 (9.7%)	1401 (6.9%)	1327 (1.3%)	1436 (9.6%)	1310
	1113 (14.7%)	1031 (6.3%)	1052 (8.4%)	1050 (8.3%)	1007 (3.8%)	961 (0.9%)	1110 (4.1%)	970
	922 (0.2%)	859 (7.0%)	864 (6.5%)	826 (10.6%)	832 (10.0%)	929 (0.5%)	914 (1.1%)	924
	863 (13.5%)	738 (2.9%)	846 (11.4%)	786 (3.4%)	816 (7.4%)	789 (3.8%)	750 (1.3%)	760
	414 (3.5%)	390 (2.4%)	400 (0.1%)	390 (2.4%)	358 (10.5%)	385 (3.8%)	362 (9.5%)	400
h_u	1905 (22.2%)	1762 (13.0%)	1791 (14.9%)	1784 (14.5%)	1646 (5.6%)	1552 (0.4%)	1709 (9.6%)	1559
	1597 (15.3%)	1447 (4.5%)	1487 (7.4%)	1491 (7.7%)	1469 (6.1%)	1385 (0.0%)	1467 (5.9%)	1385
	1453 (30.0%)	1320 (18.2%)	1353 (21.2%)	1354 (21.2%)	1269 (13.6%)	1129 (1.1%)	1344 (20.3%)	1117
	886 (10.5%)	793 (1.0%)	858 (7.1%)	824 (2.8%)	812 (1.4%)	801 (0.0%)	822 (2.6%)	801
	777 (11.7%)	753 (8.2%)	761 (9.3%)	738 (6.0%)	724 (4.0%)	700 (0.6%)	706 (1.4%)	696
	640 (13.6%)	587 (4.2%)	613 (8.9%)	592 (5.2%)	531 (5.7%)	543 (3.6%)	546 (3.0%)	563
	463 (35.0%)	455 (32.7%)	454 (32.4%)	442 (28.7%)	403 (17.5%)	361 (5.0%)	403 (17.5%)	343
t_{1u}	1637 (14.5%)	1553 (8.6%)	1587 (11.0%)	1549 (8.4%)	1437 (0.6%)	1450 (1.5%)	1628 (13.9%)	1429
	1396 (18.0%)	1245 (5.2%)	1287 (8.8%)	1297 (9.6%)	1212 (2.5%)	1208 (2.1%)	1353 (14.4%)	1183
	656 (13.9%)	614 (6.5%)	623 (8.1%)	625 (8.5%)	637 (10.6%)	589 (2.3%)	719 (24.8%)	576
	627 (18.9%)	575 (9.1%)	621 (17.8%)	599 (13.6%)	544 (3.2%)	505 (4.2%)	577 (9.5%)	527
t_{2u}	1828 (15.9%)	1709 (8.4%)	1728 (9.5%)	1713 (8.6%)	1558 (1.2%)	1575 (0.1%)	1687 (7.0%)	1577
	1327 (29.3%)	1214 (1.1%)	1259 (4.5%)	1257 (4.7%)	1241 (3.3%)	1212 (0.9%)	1314 (9.4%)	1201
	1074 (4.7%)	995 (3.1%)	1025 (0.1%)	1014 (1.2%)	999 (2.6%)	1025 (0.1%)	1134 (10.5%)	1026
	835 (22.8%)	765 (12.6%)	830 (22.1%)	799 (17.5%)	690 (1.5%)	677 (0.4%)	776 (14.1%)	680
	393 (10.5%)	377 (5.9%)	385 (8.0%)	372 (4.5%)	350 (1.7%)	367 (3.1%)	348 (2.2%)	356

MP2/DZP, and 1586 cm^{-1} and 437 cm^{-1} for MP2/TZP. Their HF calculations are in agreement with our RHF/3-21G results. Their MP2 results are more accurate when obtained with large basis sets, which also demonstrates the importance of electron correlation in predicting the vibrational frequencies.

In addition, there have been a number of second nearest-neighbor force-constant models (FCMs) (Refs. 76–78) which have been used to calculate the phonon frequencies of C_{60}. None of them yield good agreement with the experimental data. For example, an empirical force field, which has been parameterized with respect to polycyclic aromatic hydrocarbons, is used with Hückel theory and predicts vibrational frequencies of the two a_g modes of 1409 cm^{-1} and 388 cm^{-1} (Ref. 77) that are too low. However, the modified FCM (MFCM) by Jishi *et al.*[79] considered interactions up to the third-nearest neighbors, and the calculated results, as shown in Table VII, are in excellent agreement with the experiments of Wang *et al.*[25] and Dong *et al.*[26]

Table VIII also lists the vibrational frequencies of C_{60}

TABLE VIII. Vibrational frequencies $\nu(\mathrm{cm}^{-1})$ of C_{60} calculated by using B3LYP method with a variety of Pople-style basis sets. Numbers in the parentheses are the relative errors of the calculated frequencies to the experimental frequencies listed in Table VII. The approximated CPU times for STO-3G, 3-21G, 6-31G, and 6-31G* basis sets are 4 h, 5 days, 8 days, and 12 days, respectively. The other theoretical results are from Bohnen *et al.* (Ref. 34), Dixon *et al.* (Ref. 47), Hara *et al.* (Ref. 48), and Onida *et al.* (Ref. 49).

Mode	STO-3G	3-21G	6-31G	6-31G*	Hara	Dixon	Onida	Bohnen
				Even parity				
a_g	1549 (5.4%)	1501 (2.1%)	1524 (3.7%)	1504 (2.3%)	1531 (4.1%)	1525 (3.7%)	1447 (1.6%)	1475 (0.3%)
	502 (0.9%)	491 (1.4%)	496 (0.4%)	489 (1.8%)	502 (0.8%)	499 (0.2%)	482 (3.2%)	481 (3.4%)
g_g	1594 (4.5%)	1524 (0.1%)	1546 (1.4%)	1538 (0.9%)	1538 (0.9%)	1548 (1.5%)	1479 (3.0%)	1501 (1.6%)
	1380 (1.8%)	1323 (2.4%)	1342 (1.0%)	1334 (1.6%)	1337 (1.4%)	1347 (0.7%)	1314 (3.1%)	1287 (5.1%)
	1127 (4.7%)	1062 (1.3%)	1099 (2.1%)	1093 (1.6%)	1123 4.4(%)	1122 (4.3%)	1047 (2.7%)	1037 (3.6%)
	788 (2.2%)	690(14.4%)	777 (3.7%)	754 (6.5%)	759 (5.8%)	788 (2.2%)	781 (3.1%)	772 (4.2%)
	592 (4.6%)	598 (3.7%)	594 (4.3%)	577 (7.1%)	579 (6.8%)	573 (7.7%)	594 (4.3%)	570 (8.2%)
	508 (4.6%)	484 (0.4%)	500 (2.9%)	489 (0.7%)	486 (0.0%)	484 (0.4%)	482 (0.8%)	480 (1.2%)
h_g	1677 (6.3%)	1609 (2.0%)	1627 (3.1%)	1618 (2.5%)	1609 (2.0%)	1618 (2.5%)	1573 (0.3%)	1580 (0.1%)
	1500 (5.1%)	1436 (0.6%)	1466 (2.8%)	1455 (1.9%)	1475 (3.4%)	1475 (3.4%)	1394 (2.3%)	1422 (0.4%)
	1332 (6.5%)	1231 (1.6%)	1274 (1.8%)	1275 (1.9%)	1288 (3.0%)	1297 (3.7%)	1208 (3.4%)	1198 (4.2%)
	1166 (5.9%)	1112 (1.0%)	1129 (2.6%)	1125 (2.2%)	1129 (2.5%)	1128 (2.5%)	1098 (0.3%)	1079 (2.0%)
	802 (3.5%)	781 (0.8%)	788 (1.7%)	766 (1.2%)	794 (2.5%)	788 (1.7%)	775 (0.0%)	763 (1.5%)
	734 (3.3%)	678 (4.7%)	738 (3.8%)	718 (0.9%)	711 (0.0%)	727 (2.3%)	730 (2.7%)	716 (0.7%)
	449 (3.7%)	429 (1.0%)	448 (3.5%)	436 (0.8%)	430 (0.7%)	431 (0.5%)	435 (0.5%)	422 (2.5%)
	271 (0.6%)	271 (0.8%)	272 (0.5%)	266 (2.7%)	269 (1.5%)	261 (4.4%)	261 (4.4%)	263 (3.7%)
t_{1g}	1357 (0.1%)	1278 (5.9%)	1303 (4.0%)	1301 (4.2%)	1305 (3.9%)	1318 (2.9%)	1284 (5.4%)	1241 (8.6%)
	865 (11.3%)	865 (11.4%)	858 (12.1%)	840 (13.9%)	842 (13.7%)	830 (15.0%)	847 (13.2%)	826 (15.4%)
	594 (18.3%)	544 (8.3%)	593 (18.1%)	576 (14.8%)	565 (12.5%)	579 (15.3%)	580 (15.5%)	563 (10.8%)
t_{2g}	1431 (5.2%)	1330 (2.2%)	1372 (0.8%)	1370 (0.7%)	1370 (0.7%)	1393 (2.4%)	1257 (7.6%)	1277 (6.1%)
	827 (9.5%)	839 (8.2%)	829 (9.3%)	804 (12.0%)	809 (11.5%)	839 (8.2%)	816 (10.7%)	800 (12.5%)
	809 (6.4%)	650 (24.9%)	766 (11.4%)	743 (14.1%)	765 (11.6%)	804 (7.1%)	789 (8.8%)	788 (8.9%)
	581 (2.5%)	586 (3.3%)	582 (2.6%)	566 (0.1%)	566 (0.2%)	551 (2.8%)	559 (1.4%)	543 (4.4%)
				Odd parity				
a_u	994 (13.0%)	1013 (11.4%)	991 (13.3%)	982 (14.1%)	968 (15.3%)	972 (15.0%)	934 (18.3%)	973 (14.9%)
g_u	1513 (4.7%)	1435 (0.8%)	1470 (1.7%)	1461 (1.0%)	1474 (1.9%)	1480 (2.4%)	1395 (3.5%)	1420 (1.8%)
	1381 (5.4%)	1303 (0.5%)	1338 (2.1%)	1333 (1.7%)	1345 (2.7%)	1359 (3.7%)	1289 (1.6%)	1259 (3.9%)
	1009 (4.1%)	972 (0.2%)	985 (1.5%)	977 (0.7%)	989 (2.0%)	984 (1.4%)	939 (3.2%)	937 (3.4%)
	815 (11.8%)	795 (14.0%)	788 (14.7%)	787 (14.8%)	780 (15.6%)	830 (10.2%)	796 (13.9%)	790 (14.5%)
	784 (3.1%)	666 (12.4%)	775 (2.0%)	751 (1.2%)	762 (0.3%)	762 (0.3%)	763 (0.4%)	756 (0.5%)
	368 (8.1%)	359 (10.3%)	366 (8.4%)	357 (10.7%)	355 (11.3%)	350 (12.5%)	352 (12.0%)	348 (13.0%)
h_u	1668 (7.0%)	1596 (2.4%)	1617 (3.7%)	1608 (3.2%)	1598 (2.5%)	1611 (3.3%)	1545 (0.9%)	1566 (0.4%)
	1427 (3.0%)	1340 (3.2%)	1371 (1.0%)	1369 (11.8%)	1371 (1.0%)	1389 (0.3%)	1314 (5.1%)	1291 (6.8%)
	1295 (16.0%)	1219 (9.1%)	1246 (11.6%)	1243 (11.3%)	1243 (11.3%)	1248 (11.7%)	1198 (7.3%)	1175 (5.2%)
	771 (3.7%)	719 (10.3%)	763 (4.7%)	736 (8.1%)	742 (7.4%)	762 (4.9%)	769 (4.0%)	750 (6.4%)
	696 (0.1%)	674 (3.2%)	697 (0.1%)	679 (2.5%)	677 (2.7%)	671 (3.6%)	672 (3.4%)	661 (5.0%)
	564 (0.1%)	532 (5.5%)	555 (1.4%)	540 (4.1%)	537 (4.6%)	541 (3.9%)	540 (4.1%)	527 (6.4%)
	417 (21.5%)	419 (22.1%)	418 (21.8%)	408 (19.0%)	411 (19.8%)	401 (16.9%)	404 (17.8%)	388 (13.1%)
t_{1u}	1505 (5.3%)	1454 (1.7%)	1479 (3.5%)	1464 (2.4%)	1489 (4.2%)	1486 (4.0%)	1399 (2.1%)	1457 (2.0%)
	1266 (7.0%)	1175 (0.6%)	1209 (2.2%)	1212 (2.5%)	1222 (3.3%)	1224 (3.5%)	1158 (2.1%)	1143 (3.4%)
	596 (3.4%)	582 (0.9%)	587 (1.8%)	570 (1.0%)	595 (3.3%)	591 (2.6%)	566 (1.7%)	569 (1.2%)
	546 (3.6%)	508 (3.6%)	553 (4.9%)	537 (1.8%)	528 (0.2%)	535 (1.5%)	541 (2.7%)	514 (2.5%)
t_{2u}	1622 (2.8%)	1568 (0.6%)	1579 (0.2%)	1568 (0.6%)	1568 (0.6%)	1571 (0.4%)	1537 (2.5%)	1546 (2.0%)
	1235 (2.8%)	1163 (3.2%)	1201 (0.0%)	1199 (0.2%)	1231 (2.5%)	1234 (2.7%)	1108 (7.7%)	1131 (5.8%)
	1002 (2.4%)	964 (6.0%)	984 (4.1%)	966 (5.9%)	997 (2.8%)	996 (2.9%)	936 (8.8%)	945 (7.9%)
	734 (7.9%)	678 (0.3%)	742 (9.2%)	722 (6.1%)	715 (5.1%)	726 (6.8%)	774 (13.8%)	725 (6.6%)
	354 (0.5%)	345 (3.1%)	352 (4.3%)	342 (4.0%)	343 (3.7%)	342 (3.9%)	340 (4.5%)	343 (3.8%)

calculated by other DFT methods, for example, LDA-PPA,[34] LDA,[47,48] and DFT-LDA-based CPMD simulations.[49] In general, those calculated results are in good agreement with experiment. Very recently, Choi *et al.*[80] have performed B3LYP vibrational calculations of C_{60} with a 3-21G basis set but involving scaling of the internal force constants (SIFC) $\tilde{K}_{ij}^{\mathrm{int}}$ by using Pulay's method,[81] i.e., $\tilde{K}_{ij}^{\mathrm{scaled}}=(s_i s_j)^{1/2}\tilde{K}_{ij}^{\mathrm{int}}$, where $\tilde{K}_{ij}^{\mathrm{int}}$ is the force constant in internal coordinates (the GAUSSIAN 98 program[30] uses this form), and s_i and s_j are scaling factors for the ith and jth redundant internal coordinates, respectively. They optimized the scaling factors by minimizing the root-mean-square deviations between the experimental and calculated scaled frequencies. Their results are listed in Table IX. Overall, their scaling procedure improves the accuracy for the 46 vibrational frequencies of C_{60}, especially, for the a_g, h_g, and t_{1u} vibrational modes.

We calculated the vibrational frequencies for $C_{48}N_{12}$ by using RHF and B3LYP methods with a variety of Pople-style basis sets. In contrast with C_{60}, it is found that there are in total 116 vibrational modes for $C_{48}N_{12}$ because of its lowered

TABLE IX. Vibrational frequencies $\nu\,(\mathrm{cm}^{-1})$ of C_{60} obtained by Choi *et al.* (Ref. 80) using B3LYP/3-21G but involving scaling of the internal force constant by using Pulay's method. Numbers in the parentheses are the relative errors of the calculated frequencies to the experimental frequencies listed in Table VII.

Even parity						Odd parity					
Mode	ν	Mode	ν	Mode	ν	Mode	ν	Mode	ν	Mode	ν
a_g	1470(0.0%)			t_{1g}	290 (5.0%)	a_u	1078 (5.7%)			t_{1u}	1433 (0.3%)
	495(0.6%)	h_g	1576 (0.1%)		904 (7.4%)						1180 (0.3%)
			142 (0.0%)		565 (12.5%)			h_u	1567 (0.5%)		577 (0.2%)
g_g	1497(1.8%)		1251 (0.0%)			g_u	1429 (1.2%)		1343 (3.0%)		526 (0.2%)
	1348(0.6%)		1101 (0.0%)				1315 (0.4%)		1214 (8.7%)	t_{2u}	1524 (3.4%)
	1040(3.3%)		775 (0.0%)	t_{2g}	1340 (1.5%)		970 (0.0%)		737 (8.0%)		1142 (5.0%)
	758(6.0%)		711 (0.0%)		831 (9.1%)		797 (13.7%)		694 (0.3%)		955 (6.9%)
	592(4.7%)		431 (0.5%)		668 (22.8%)		707 (7.0%)		535 (5.0%)		716 (5.3%)
	485(0.2%)		267 (2.2%)		614 (8.3%)		354 (11.5%)		403(17.5%)		340 (4.5%)

symmetry, S_6. These vibrational modes are classified into 58 doubly-degenerate and 58 nondegenerate modes. Among those vibrational modes, there are 58 IR-active and 58 Raman-active modes. We also found that the electron correlation or increasing the basis size results in a redshift of the vibrational frequencies. In detail, Tables X and XI list the IR- and Raman-active modes of $C_{48}N_{12}$ calculated with B3LYP/3-21G and B3LYP/6-31G*.

B. IR Intensities in $C_{48}N_{12}$ and C_{60}

We perform calculations of IR intensities I_{IR} (Ref. 82) for both $C_{48}N_{12}$ and C_{60} by using the GAUSSIAN 98 program[30,31] with RHF and B3LYP methods. The calculated IR intensities for C_{60} at the corresponding frequencies are listed in Table XII, and those for $C_{48}N_{12}$ are shown in Fig. 4.

For C_{60}, we note that its IR spectrum is very simple. Namely, it is composed of 4 IR-active vibrational modes with t_{1u} symmetry. From Table XII, we see that the IR intensity of a given mode decreases due to the electron correlation and converges with increasing basis size. We find that our intensities calculated with B3LYP agree reasonably with experimental spectrum[83] obtained by *in situ* high-resolution FTIR measurement of a C_{60} film.

The IR intensities I_{IR} at the corresponding vibrational

TABLE X. Fifty eight IR-active frequencies (ν, in cm^{-1}) of $C_{48}N_{12}$ calculated by using B3LYP methods with 3-21G and 6-31G* basis sets.

Doubly-degenerate modes		Nondegenerate modes	
B3LYP/3-21G	B3LYP/6-31G*	B3LYP/3-21G	B3LYP/6-31G*
308	309	287	287
359	357	318	325
404	395	359	360
412	406	402	395
422	425	413	431
440	446	454	460
469	481	567	579
558	570	600	611
585	606	609	622
635	639	654	645
665	658	698	686
686	675	709	700
701	695	798	778
721	712	809	786
804	782	963	961
958	954	977	967
1041	1040	1010	976
1136	1159	1042	1047
1172	1197	1142	1177
1210	1237	1215	1229
1280	1302	1252	1270
1311	1340	1293	1317
1354	1389	1345	1384
1410	1437	1374	1394
1443	1473	1381	1418
1475	1499	1418	1461
1521	1553	1497	1518
1544	1576	1516	1555
1592	1624	1542	1575

TABLE XI. Fifty eight Raman-active frequencies (ν, in cm^{-1}) for $C_{48}N_{12}$ calculated by using B3LYP methods with 3-21G and 6-31G* basis sets.

Doubly-degenerate modes		Nondegenerate modes	
B3LYP/3-21G	B3LYP/6-31G*	B3LYP/3-21G	B3LYP/6-31G*
248	245	264	264
261	260	368	376
368	371	398	398
388	396	415	424
429	437	458	467
450	472	491	495
568	551	505	510
596	581	588	576
613	627	598	588
629	641	603	597
671	671	614	627
695	699	657	656
760	766	690	689
776	780	765	766
865	843	851	830
887	854	881	844
1084	1093	1080	1092
1123	1138	1160	1162
1147	1156	1181	1189
1186	1223	1241	1265
1243	1272	1253	1279
1311	1336	1293	1320
1369	1404	1347	1379
1388	1420	1373	1397
1415	1451	1419	1441
1489	1515	1440	1477
1516	1551	1487	1505
1544	1578	1509	1530
1578	1610	1592	1623

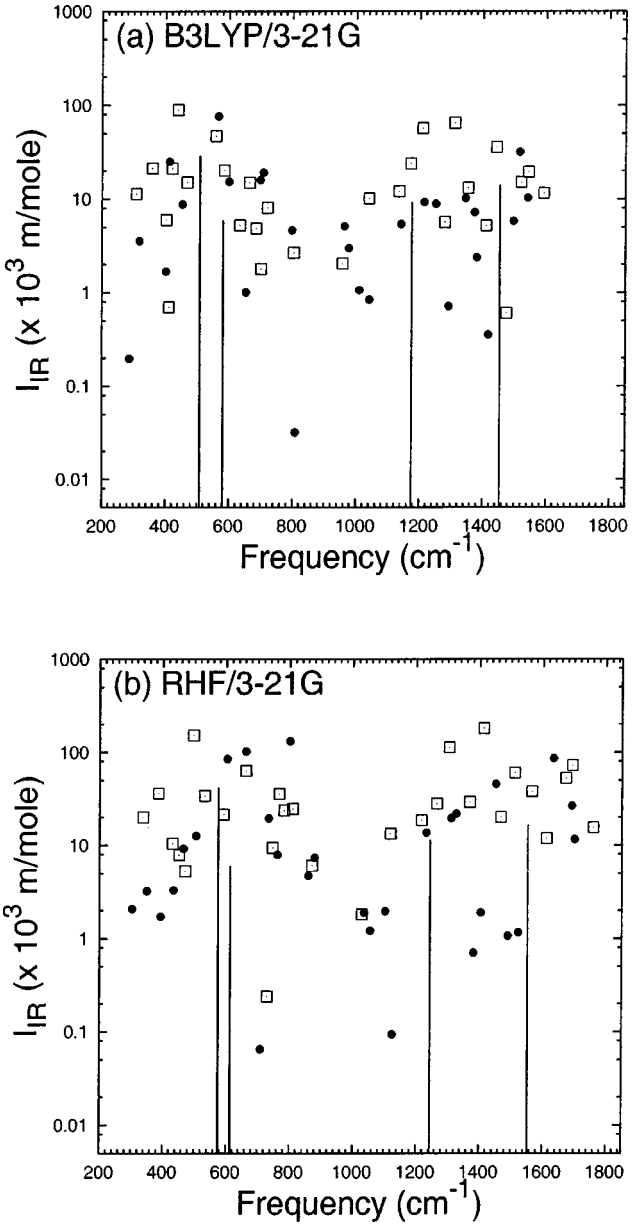

FIG. 4. *Ab initio* calculation of IR intensity (I_{IR}, in 10^3 m/mol) for C_{60} (solid line) and $C_{48}N_{12}$ (filled circles: nondegenerated; open squares: doubly-degenerate): (a) B3LYP/3-21G and (b) RHF/3-21G.

frequencies for $C_{48}N_{12}$ are presented in Figs. 4(a) and 4(b) for calculations with B3LYP/3-21G and RHF/3-21G, respectively. As discussed above, $C_{48}N_{12}$ has 29 nondegenerate and 29 doubly-degenerate IR-active vibrational modes. Similar to the case of C_{60}, the IR signals separate into two regions, i.e.,

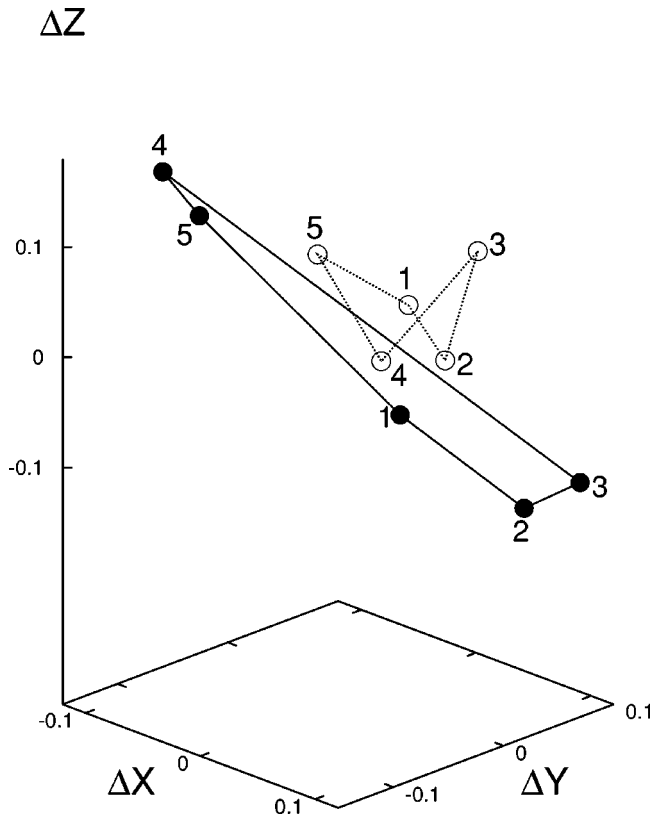

FIG. 5. The vibrational displacements of sites 1–5 for the strongest IR spectral signals in both low-frequency (filled circles) and high-frequency (open circles) regions of $C_{48}N_{12}$ for the B3LYP/3-21G case.

a high-frequency ($>1000\ cm^{-1}$) and a low-frequency ($\leqslant 1000\ cm^{-1}$) region. The IR-active frequencies are red shifted by including the electron correlation or increasing the basis size (the results are not presented here). We found that the IR intensities decrease after including electron correlations and converge with increasing basis size. The strongest IR spectral lines in both low- and high-frequency regions are the doubly-degenerate modes located, for example, at $440\ cm^{-1}$ and $1310\ cm^{-1}$, respectively, for the B3LYP/3-21G case. Since experimental IR spectroscopic data do not directly indicate the specific type of nuclear motion producing each IR peak, we do not give here the normal mode information for each vibrational frequency and the displacements of each nuclei corresponding to each normal mode. In Fig. 5, taking B3LYP/3-21G calculations as an example, we only show the vibrational displacements of sites 1–5 (4 C sites and 1 N site) for the strongest IR spectral signals in the low- and high-frequency regions. It is seen that the pentagon

TABLE XII. RHF and B3LYP calculations of IR intensities (I_{IR}, in 10^3 m/mol) of C_{60} with the corresponding vibrational modes and frequencies (ν, in cm^{-1}).

	B3LYP/3-21G		B3LYP/6-31G		B3LYP/6-31G*		RHF/6-31G*	
Mode	I_{IR}	ν	I_{IR}	ν	I_{IR}	ν	I_{IR}	ν
t_{1u}	14.0	1454	17.2	1479	15.6	1464	17.1	1549
	9.2	1175	10.1	1209	8.9	1212	10.6	1297
	5.9	582	8.2	587	10.7	570	10.4	625
	28.8	508	27.7	553	27.1	537	48.0	599

TABLE XIII. RHF and B3LYP calculations of the absolute isotropy (σ, in ppm) and anisotropy ($\Delta\sigma$, in ppm) of the carbon and nitrogen shielding tensors with a variety of Pople-style basis sets for $C_{48}N_{12}$ aza-fullerene, C_{60} and tetramethylsilane (TMS) by using GIAO method. Numbers in the parentheses for C_{60} are the relative errors of the calculated ^{13}C NMR shift δ to the NMR chemical shift $\delta^{exp}=142.7$ ppm measured by Taylor *et al.* (Ref. 86).

				STO-3G		6-31G		6-31G*	
Method	Molecule	Site numbers $\{n_i\}$	Nuclei	σ	$\Delta\sigma$	σ	$\Delta\sigma$	σ	$\Delta\sigma$
RHF	$C_{48}N_{12}$	{1, 13, 16, 31, 38, 51}	^{13}C	91.5	155.5	44.0	173.0	48.5	168.3
		{2, 12, 29, 32, 37, 52}	^{13}C	109.8	156.7	67.9	169.2	67.7	168.2
		{3, 11, 28, 33, 36, 53}	^{13}C	116.8	132.2	76.6	141.2	88.5	126.9
		{4, 15, 27, 34, 40, 54}	^{13}C	103.5	141.9	57.9	154.9	46.9	156.7
		{5, 14, 30, 35, 39, 55}	^{15}N	193.7	134.8	114.4	171.5	140.7	128.5
		{6, 18, 24, 42, 48, 58}	^{13}C	120.2	104.8	78.2	110.5	89.6	82.5
		{7, 19, 23, 43, 47, 57}	^{13}C	106.2	135.9	59.4	152.2	54.2	148.7
		{8, 20, 22, 44, 46, 56}	^{13}C	111.5	140.9	70.7	150.8	82.9	131.1
		{9, 21, 26, 45, 50, 60}	^{15}N	182.7	151.6	95.3	202.6	121.7	170.4
		{10, 17, 25, 41, 49, 59}	^{13}C	104.9	125.2	59.5	133.5	55.1	126.9
	C_{60}	{1, 2, 3, 4, 5, 6, ..., 60}	^{13}C	101.8	156.6	54.1	180.1	54.7	178.8
	TMS	carbon site	^{13}C	238.5	5.6	200.8	21.4	195.1	17.5
	NH_3	nitrogen site	^{15}N	306.9	9.2	264.4	18.2	260.8	17.4
	C_{60}	Calculated ^{13}C NMR shift δ		136.7 (4.2%)		146.7 (2.8%)		140.4 (1.6%)	
B3LYP	$C_{48}N_{12}$	{1, 13, 16, 31, 38, 51}	^{13}C	103.9	109.5	53.3	128.0	51.9	130.4
		{2, 12, 29, 32, 37, 52}	^{13}C	114.6	121.9	66.4	138.1	62.8	138.9
		{3, 11, 28, 33, 36, 53}	^{13}C	120.6	101.1	74.5	110.9	72.9	107.3
		{4, 15, 27, 34, 40, 54}	^{13}C	113.3	103.6	66.3	117.1	61.8	113.9
		{5, 14, 30, 35, 39, 55}	^{15}N	173.2	126.2	92.8	155.4	103.8	139.3
		{6, 18, 24, 42, 48, 58}	^{13}C	123.5	70.4	76.1	76.4	74.3	63.0
		{7, 19, 23, 43, 47, 57}	^{13}C	114.1	96.4	63.0	76.4	57.4	114.0
		{8, 20, 22, 44, 46, 56}	^{13}C	119.5	101.7	73.8	116.2	72.3	116.2
		{9, 21, 26, 45, 50, 60}	^{15}N	171.7	121.9	84.0	157.5	91.2	146.7
		{10, 17, 25, 41, 49, 59}	^{13}C	113.9	121.9	65.6	94.4	61.7	90.0
	C_{60}	{1, 2, 3, 4, 5, 6, ..., 60}	^{13}C	106.1	125.8	53.6	152.2	50.5	154.2
	TMS	carbon site	^{13}C	225.3	9.6	188.3	25.2	183.8	22.3
	NH_3	nitrogen site	^{15}N	291.3	7.3	256.8	21.0	254.9	19.3
	C_{60}	Calculated ^{13}C NMR shift δ		119.2 (16.5%)		134.7 (5.6%)		133.3 (6.6%)	

structure for the low-frequency case expands slightly and shows collective vibration along the $z-x$ direction, while the pentagon structure for the high-frequency case contracts, accompanying a large stretching of site 3 along the z direction.

VI. NUCLEAR MAGNETIC SHIELDING TENSORS

The nuclear magnetic shielding isotropy σ is defined as $\sigma=(\sigma_{xx}+\sigma_{yy}+\sigma_{zz})/3$,[29] where σ_{ij} $(i,j=x,y,z)$ is the component of the shielding tensor. The shielding anisotropy $\Delta\sigma$, an indication of the quality of the magnetic shielding tensor, is defined as $\Delta\sigma=\sigma_3-(\sigma_1+\sigma_2)/2$,[29] where $\sigma_1<\sigma_2<\sigma_3$ are the eigenvalues of the shielding tensor. The nuclear magnetic shielding difference, or say, *chemical shift* δ, is reported in ppm (i.e., parts per million) and given by $\delta=(\sigma^r-\sigma^s)\times10^6$,[27] where σ^r and σ^s denote the shielding isotropies σ for the reference and sample, respectively. There are a number of theoretical methods for calculating the second-order magnetic response properties of molecules. In this paper, we focus on using two gauge-invariant procedures, i.e., the gauge-including atomic orbital (GIAO) procedure and the continuous set of gauge transformations (CSGT) procedure, to predict NMR shielding tensors at the RHF and DFT levels of theory. GIAO and CSGT achieve gauge-invariance in different ways: the GIAO method uses basis functions having explicit field dependence,[84] whereas the CSGT method achieves the gauge-invariance by performing a continuous set of gauge transformations.[29] Both GIAO and CSGT methods have been implemented into the GAUSSIAN 98 program.[30,31] All calculations in this section are performed using this program.

Here we perform RHF and B3LYP hybrid DFT calculations of the nuclear magnetic shielding tensor of carbon and nitrogen atoms in $C_{48}N_{12}$, C_{60}, and tetramethylsilane [TMS (Ref. 85)] by using GIAO and CSGT methods. Calculation performed with a specific basis set and *ab initio* method use geometry optimized with the same basis set and *ab initio* method (see Sec. II). Detailed results are summarized in Table XIII and XIV. Since no present functional includes a magnetic field dependence, the DFT methods do not provide systematically better shielding results than the RHF.[30] Nevertheless, we also list the DFT results in Table XIII and XIV for comparison. The isotropic ^{13}C NMR chemical shifts δ relative to that of TMS are also shown in Table XIII and XIV. It is seen that eight ^{13}C and two ^{15}N NMR spectral signals are predicted for $C_{48}N_{12}$. In contrast, C_{60} has only one ^{13}C NMR signal which is in agreement with experiment.[86] The experimental values of the absolute shielding constant σ for ^{15}N in NH_3 and ^{13}C in TMS are 264.5 ppm (Refs. 87, 88) and 188.1 ppm.[85] From Tables XIII and XIV, we find that our best calculated results for those reference materials are in good agreement with the experiments.

Table XIII and XIV also demonstrate the convergence of the GIAO and CSGT methods with respect to basis set for

TABLE XIV. RHF and B3LYP calculations of the absolute isotropy (σ, in ppm) and anisotropy ($\Delta\sigma$, in ippm) of the carbon and nitrogen shielding tensors with a variety of Pople-style basis sets for $C_{48}N_{12}$ aza-fullerene, C_{60} and tetramethylsilane (TMS) by using CSGT methods. Numbers in the parentheses for C_{60} are the relative errors of the calculated ^{13}C NMR shift δ to the NMR chemical shift $\delta^{exp}=142.7$ ppm measured by Taylor *et al.* (Ref. 86).

				STO-3G		6-31G		6-31G*	
Method	Molecule	Site numbers $\{n_i\}$	Nuclei	σ	$\Delta\sigma$	σ	$\Delta\sigma$	σ	$\Delta\sigma$
RHF	$C_{48}N_{12}$	{1, 13, 16, 31, 38, 51}	^{13}C	45.3	125.0	30.7	168.9	41.3	170.1
		{2, 12, 29, 32, 37, 52}	^{13}C	55.8	127.0	54.0	162.1	60.4	168.3
		{3, 11, 28, 33, 36, 53}	^{13}C	60.0	114.0	60.9	139.1	78.9	129.8
		{4, 15, 27, 34, 40, 54}	^{13}C	52.9	119.5	41.1	155.5	39.2	160.4
		{5, 14, 30, 35, 39, 55}	^{13}N	78.0	134.0	86.3	176.5	128.2	136.4
		{6, 18, 24, 42, 48, 58}	^{13}C	63.8	97.9	59.3	115.5	79.8	87.3
		{7, 19, 23, 43, 47, 57}	^{13}C	55.5	113.5	43.2	149.5	46.5	150.5
		{8, 20, 22, 44, 46, 56}	^{13}C	58.6	118.0	52.4	150.1	73.7	135.2
		{9, 21, 26, 45, 50, 60}	^{13}N	74.0	144.8	72.2	203.6	112.2	173.1
		{10, 17, 25, 41, 49, 59}	^{13}C	55.3	107.8	43.3	136.9	47.3	129.5
	C_{60}	{1, 2, 3, 4, 5, 6, ..., 60}	^{13}C	50.2	128.8	43.3	172.7	48.9	178.6
	TMS	carbon site	^{13}C	131.9	9.5	185.5	13.1	190.6	13.7
	NH_3	nitrogen site	^{13}N	148.1	18.6	209.2	6.3	228.4	6.6
	C_{60}	Calculated ^{13}C NMR shift δ		81.7 (42.7%)		142.2 (0.4%)		141.7 (0.7%)	
B3LYP	$C_{48}N_{12}$	{1, 13, 16, 31, 38, 51}	^{13}C	58.6	86.4	39.1	126.6	45.7	131.8
		{2, 12, 29, 32, 37, 52}	^{13}C	66.1	94.8	53.9	133.5	57.2	139.6
		{3, 11, 28, 33, 36, 53}	^{13}C	69.3	83.5	60.3	111.1	66.3	109.4
		{4, 15, 27, 34, 40, 54}	^{13}C	64.6	84.8	49.1	118.5	54.7	117.6
		{5, 14, 30, 35, 39, 55}	^{13}N	78.5	116.6	74.6	152.7	96.8	142.4
		{6, 18, 24, 42, 48, 58}	^{13}C	71.9	63.6	58.7	81.9	66.9	66.5
		{7, 19, 23, 43, 47, 57}	^{13}C	66.5	77.7	47.5	112.2	51.0	115.3
		{8, 20, 22, 44, 46, 56}	^{13}C	70.4	81.9	56.7	115.8	65.7	118.7
		{9, 21, 26, 45, 50, 60}	^{13}N	81.6	112.8	69.3	156.6	86.0	148.5
		{10, 17, 25, 41, 49, 59}	^{13}C	66.9	71.6	49.5	100.1	54.8	93.8
	C_{60}	{1, 2, 3, 4, 5, 6, ..., 60}	^{13}C	58.2	100.3	43.1	148.4	45.9	149.2
	TMS	carbon site	^{13}C	124.9	10.0	175.0	16.5	181.6	18.0
	NH_3	nitrogen site	^{13}N	137.7	27.1	200.4	6.0	221.5	6.5
	C_{60}	Calculated ^{13}C NMR shift δ		66.7 (53.3%)		131.9 (7.6%)		135.7 (4.9%)	

absolute shielding constants calculated with RHF and B3LYP hybrid DFT methods. For each first principles method, the shielding constants calculated with GIAO and CSGT methods are found to converge to almost the same values for the large basis set 6-31G*. NMR chemical shifts, as opposed to the absolute shielding constants σ, are measured with high accuracy in applications of NMR spectroscopy. On the other hand, calculated chemical shifts are in better agreement with experiment as relative differences are better represented.[29] Hence, given the absolute shielding constants for ^{13}C and ^{15}N in reference materials, i.e., TMS and NH_3 shown in Table XIII and XIV, we are able to calculate the chemical shifts δ and compare them with the experiments. For C_{60}, we find that the NMR chemical shifts δ calculated with the CSGT method at the RHF/6-31G and RHF/6-31G* levels are in agreement with experiment ($\delta^{exp}=142.7$ ppm measured by Taylor *et al.*[86]). This suggests that CSGT method would predict NMR spectral signals much better than GIAO. However, CSGT costs more CPU times than GIAO on the same machine, for example, about 5 h more for RHF/6-31G* and 2 h for B3LYP/6-31G* in the CSGT method.

To predict accurate NMR chemical shifts for large molecules, it is necessary to assess the accuracy of the available *ab initio* methods by employing lower levels of theory and by using basis sets as small as possible.[29] The results in Tables XIII and XIV indicate that the RHF method yields better chemical shifts than the B3LYP hybrid DFT method, especially, for the GIAO method and the minimum basis set STO-3G. As shown in Table XIII, the ^{13}C chemical shift in C_{60} for the minimum basis set STO-3G differs from experiment by 23.5 ppm at the B3LYP level, but by only 6 ppm at the RHF level. Also it is noted that RHF makes positive and negative errors, while B3LYP makes only positive errors.

In addition, nuclear magnetic shielding anisotropies $\Delta\sigma$ are reported in Tables XIII and XIV. Although these properties usually cannot be determined experimentally in the gas phase (except in cases where the high symmetry of the molecule together with the calculated diamagnetic contribution to the shielding tensor allows the determination of the anisotropy from the spin rotation[89]), these values are of interest. Anisotropies can be determined in solid state NMR experiments and calculations are often important for a correct assignment. From Tables XIII and XIV, we find that the shielding anisotropies $\Delta\sigma$ for ^{15}N in NH_3 calculated with GIAO method with both *ab initio* theories are in good agreement with experiment [$\Delta\sigma=20$ (Refs. 87, 88)], while those calculated with CSGT agree poorly with experiment.

VII. SUMMARY AND OUTLOOK

In summary, we have performed *ab initio* calculations of the structures, electronic properties, vibrational frequencies, IR intensities, NMR shielding tensors, linear polarizabilities,

and second-order hyperpolarizabilities of the $C_{48}N_{12}$ azafullerene. Calculated results of $C_{48}N_{12}$ are compared to those of C_{60} at the same level of theory. It is found that this azafullerene has some remarkable features, which are different from and can compete with C_{60}. The detailed studies of C_{60} show the importance of electron correlations and the choice of basis sets in the *ab initio* calculations. Our best results for C_{60} obtained with the B3LYP hybrid DFT method are in excellent agreement with experiment and demonstrate the needed efficiency and accuracy of this method for obtaining quantitative information on the structural, electronic, and vibrational properties of these materials.

Laser sources are widely used in the laboratory and industry. However, they are a potential hazard for eyes, thermal cameras and other optical sensors.[4,5] Development of ideal optical limiters which can suppress undesired radiation and effectively decrease transmittance at high intensity or fluence is necessary. C_{60} and fullerene derivatives are good candidates for optical limiting applications.[4] In this paper, we found that the average second-order hyperpolarizability of $C_{48}N_{12}$ is about 55% larger than that of C_{60}. Hence, it is expected that $C_{48}N_{12}$ is also a good candidate for optical limiting applications.

Nonlinear optical (NLO) materials have vast technological applications in telecommunications, optical data storage and optical information processing. The search for such NLO materials is the subject of intense research.[3,4] Based on such donor–acceptor model,[4] we can link donor $C_{48}N_{12}$ and acceptor C_{60} with a polyene or an aromatic chain and design one kind of organic molecules. In such organic molecules, charge would migrate from $C_{48}N_{12}$ to C_{60} upon electronic excitation, giving rise to a large dipole moment along the direction connecting the donor/acceptor pair. Thus, large NLO response is expected in these donor/acceptor-based molecules.

Carbon nanotubes are promising materials for building electronic devices, in particular, field effect transistors (FETs).[5] However, single-walled carbon nanotube (SWNT) FETs built from as-grown tubes are unipolar p-type, i.e., there is no electron current flow even at large positive gate biases. Obviously, the capability to produce n-type transistors is important technologically, as it allows the fabrication of nanotube-based complementary logic devices and circuits.[5] As shown in this paper, $C_{48}N_{12}$ is a good electron donor. We found that incorporating $C_{48}N_{12}$ into a (10,10) semiconducting SWNT (Ref. 2) would result in $-0.26\,e$ charge[37] on the nanotube forming a n-type SWNT-based transistor. Thus this opens a way to making nanotube-based n-type transistors or $p-n$ junctions by using $C_{48}N_{12}$.

To obtain molecular rectification, the LUMO of the acceptor should lie at or slightly above the Fermi level of the electrode and above the HOMO of the donor.[90] Hence it is important to search for desired donor/acceptor pairs which satisfy those conditions. The acceptor/donor pair, $C_{48}B_{12}$/$C_{48}N_{12}$, actually is demonstrated to be an ideal candidate for molecular electronics.[37] For example, we have shown that a molecular rectifier built by $C_{48}B_{12}/C_{48}N_{12}$ pair shows a perfect rectification behavior.[37]

As shown before, $C_{48}B_{12}$ and $C_{48}N_{12}$ molecules have opposite electronic polarizations and their fcc solids are semiconducting materials. Hence, it is possible to use them to build semiconducting materials with opposite electronic polarizations.

Therefore, $C_{48}N_{12}$ could have potential applications as semiconductor components, nonlinear optical materials, and possible building materials for molecular electronics and photonic devices. Efficiently synthesizing $C_{48}N_{12}$ would be of great experimental interest within reach of today's technology.

ACKNOWLEDGMENTS

We thank Dr. Denis A. Lehane and Dr. Hartmut Schmider for their technical help. One of us (R.H.X.) thanks the HPCVL at Queen's University for the use of its parallel supercomputing facilities. L.J. gratefully acknowledges the Danish Research Training Council for financial support. J.Z. acknowledges support from the University Research Council of University of North Carolina at Chapel Hill. V.H.S. gratefully acknowledges support from the Natural Science and Engineering Research Council of Canada (NSERC).

[1] W. Krätschmer, L. D. Lamb, K. Fostiropoulos, and D. R. Huffman, Nature (London) **347**, 354 (1990).
[2] M. S. Dresselhaus, G. Dresselhaus, and P. C. Eklund, *Science of Fullerenes and Carbon Nanotubes* (Academic, New York, 1996).
[3] R. H. Xie, ''Nonlinear optical properties of fullerenes and carbon nanotubes,'' in *Handbook of Advanced Electronic and Photonic Materials and Devices*, edited by H. S. Nalwa (Academic, New York, 2000), Vol. 9, pp. 267–307.
[4] R. H. Xie, Q. Rao, and L. Jensen, ''Nonlinear optics of fullerenes and carbon nanotubes,'' in *Encyclopedia of Nanoscience and Nanotechnology*, edited by H. S. Nalwa (American Scientific Publisher, California, 2003).
[5] R. H. Xie, J. Zhao, and Q. Rao, ''Doped carbon nanotubes,'' in *Encyclopedia of Nanoscience and Nanotechnology*, edited by H. S. Nalwa (American Scientific Publisher, California, 2003).
[6] T. Guo, C. M. Jin, and R. E. Smalley, J. Phys. Chem. **95**, 4948 (1991).
[7] J. C. Hummelen, B. Knight, J. Pavlovich, R. González, and F. Wudl, Science **269**, 1554 (1995).
[8] W. Andreoni, A. Curioni, K. Holczer, K. Prassides, M. Keshavarz-K, J. C. Hummelen, and F. Wudl, J. Am. Chem. Soc. **118**, 11335 (1996).
[9] L. Hultman, S. Stafström, Z. Czigány, J. Neidhardt, N. Hellgren, I. F. Brunell, K. Suenaga, and C. Cooliex, Phys. Rev. Lett. **87**, 225503 (2001).
[10] S. Stafström, L. Hultman, and N. Hellgren, Chem. Phys. Lett. **340**, 227 (2001).
[11] R. H. Xie, G. W. Bryant, and V. H. Smith, Jr., Chem. Phys. Lett. **368**, 486 (2003).
[12] J. Cioslowski, *Electronic Structure Calculations on Fullerenes and Their Derivatives* (Oxford University Press, New York, 1995).
[13] G. E. Scuseria, Science **271**, 942 (1996).
[14] P. R. Taylor, E. Bylaska, J. H. Weare, and R. Kawai, Chem. Phys. Lett. **235**, 558 (1995).
[15] R. L. Disch and J. M. Schulmann, Chem. Phys. Lett. **125**, 465 (1986).
[16] H. P. Lüthi and J. Almlöf, Chem. Phys. Lett. **135**, 357 (1987).
[17] G. Scuseria, Chem. Phys. Lett. **176**, 423 (1991).
[18] M. Häser, J. Almlöf, and G. E. Scuseria, Chem. Phys. Lett. **181**, 497 (1991).
[19] N. Kurita, K. Kobayashi, H. Kumahora, and K. Tago, Phys. Rev. B **48**, 4850 (1993).
[20] J. Hrusák and H. Schwarz, Chem. Phys. Lett. **205**, 187 (1993).
[21] D. Bakowies, M. Bühl, and W. Thiel, Chem. Phys. Lett. **247**, 491 (1995).
[22] W. Kohn and L. J. Sham, Phys. Rev. A **140**, A1133 (1965).
[23] G. E. Scuseria, Chem. Phys. Lett. **243**, 193 (1995).
[24] N. B. Colthup, L. H. Daly, and S. E. Wiberley, *Introduction to Infrared and Raman Spectroscopy*, 3rd ed. (Academic, New York, 1990).
[25] K. A. Wang, A. M. Rao, P. C. Eklund, M. S. Dresselhaus, and G. Dresselhaus, Phys. Rev. B **48**, 11375 (1993).

[26] Z. H. Dong, P. Zhou, J. M. Holden, P. C. Eklund, M. S. Dresselhaus, and G. Dresselhaus, Phys. Rev. B **48**, R2862 (1993).
[27] I. Ando and G. A. Webb, *Theory of NMR Parameters* (Academic, New York, 1983).
[28] N. S. Ramsey, Phys. Rev. **78**, 699 (1950).
[29] J. R. Cheeseman, M. J. Frisch, G. W. Trucks, and T. A. Keith, J. Chem. Phys. **104**, 5497 (1996).
[30] M. J. Frisch, G. W. Trucks, H. B. Schlegel *et al.*, GAUSSIAN 98, Revision A.9 Gaussian, Inc., Pittsburgh, PA, 1998.
[31] Use of this software does not constitute an endorsement or certification by NIST.
[32] A. D. Becke, J. Chem. Phys. **98**, 5648 (1993).
[33] H. B. Bürgi, E. Blanc, D. Schwarzenbach, S. Liu, Y. Lu, M. M. Kappes, and J. A. Ibers, Angew. Chem. Int. Ed. Engl. **41**, 640 (1992).
[34] K. P. Bohnen, R. Heid, K. M. Ho, and C. T. Chan, Phys. Rev. B **51**, 5805 (1995).
[35] Q. M. Zhang, J. Y. Yi, and J. Bernholc, Phys. Rev. Lett. **66**, 2633 (1991).
[36] A. Szabo and N. S. Ostlund, *Modern Quantum Chemistry* (Macmillan, New York, 1982).
[37] R. H. Xie, G. W. Bryant, J. Zhao, V. H. Smith, Jr., A. Di Carlo, and A. Pecchia (unpublished).
[38] W. I. F. David, R. M. Ibberson, J. C. Matthewman, K. Prassides, T. J. S. Dennis, J. P. Hare, H. W. Kroto, R. Taylor, and D. R. M. Walton, Nature (London) **353**, 147 (1991).
[39] C. S. Yannoni, P. P. Bernier, D. S. Bethune, G. Maijer, and J. R. Salem, J. Am. Chem. Soc. **113**, 3190 (1991).
[40] R. D. Johnson, G. Meijier, and D. S. Bethune, J. Am. Chem. Soc. **112**, 8983 (1990).
[41] K. Hedberg, L. Hedberg, D. S. Bethune, C. A. Brown, H. C. Dorn, R. D. Johnson, and M. de Vries, Science **254**, 410 (1991).
[42] R. C. Haddon, L. E. Brus, and K. Raghavachari, Chem. Phys. Lett. **125**, 459 (1986).
[43] F. Negri, G. Orlandi, and F. Zerbetto, Chem. Phys. Lett. **144**, 31 (1988).
[44] R. E. Stanton and M. D. Newton, J. Phys. Chem. **92**, 2141 (1988).
[45] M. Kállay, K. Németh, and P. R. Surján, J. Phys. Chem. **102**, 1261 (1998).
[46] X. Q. Wang, C. Z. Wang, and K. M. Ho, Phys. Rev. B **48**, 1884 (1993).
[47] D. A. Dixon, B. E. Chase, G. Fitzgerald, and N. Matsuzawa, J. Phys. Chem. **99**, 4486 (1995).
[48] T. Hara, J. Onoe, and K. Takeuchi, Phys. Rev. B **63**, 115412 (2001).
[49] G. Onida, W. Andreoni, J. Kohanoff, and M. Parrinello, Chem. Phys. Lett. **219**, 1 (1994).
[50] I. V. Hertel, H. Steger, J. DeVries, B. Weisser, C. Menzel, B. Kamke, and W. Kamke, Phys. Rev. Lett. **68**, 784 (1992).
[51] R. K. Yoo, B. Ruscic, and J. Berkowitz, J. Chem. Phys. **96**, 911 (1992).
[52] J. DeVries, H. Steger, B. Kamke, C. Menzel, B. Weisser, W. Kamke, and I. V. Hertel, Chem. Phys. Lett. **188**, 159 (1992).
[53] H. Steger, J. Holzapfel, A. Hielscher, W. Kamke, and I. V. Hertel, Chem. Phys. Lett. **234**, 455 (1995).
[54] C. Brink, L. H. Andersen, P. Hvelplund, D. Mathur, and J. D. Voldstad, Chem. Phys. Lett. **233**, 52 (1995).
[55] X. B. Wang, C. F. Ding, and L. S. Wang, J. Chem. Phys. **110**, 8217 (1999).
[56] R. W. Lof, M. A. van Veenendaal, B. Koopmans, H. T. Jonkman, and G. A. Sawatzky, Phys. Rev. Lett. **68**, 3924 (1992).
[57] CASTEP, distributed by Accelrys Inc., is a DFT package based on plane-wave pseudopotential technique: M. C. Payne *et al.*, Rev. Mod. Phys. **64**, 1045 (1992).
[58] R. M. Fleming, A. P. Ramirez, M. J. Rosseinsky, D. W. Murphy, R. C. Haddon, S. M. Zahurak, and A. V. Makhija, Nature (London) **352**, 787 (1991).
[59] R. Schwedhelm, L. Kipp, A. Dallmeyer, and M. Skibowski, Phys. Rev. B **58**, 13176 (1998).
[60] ADF 2002.01, Theoretical Chemistry Vrije Universiteit, Amsterdam, 2002.
[61] G. te Velde, F. M. Bickelhaupt, E. J. Baerends, C. Fonseca Guerra, S. J. A. van Gisbergen, J. G. Snijders, and T. Ziegler, J. Comput. Chem. **22**, 931 (2001).
[62] G. D. Zeiss, W. R. Scott, N. Suzuki, and D. P. Chong, Mol. Phys. **37**, 1543 (1979).
[63] L. Jensen, P. Th. van Duijnen, J. G. Snijders, and D. P. Chong, Chem. Phys. Lett. **359**, 524 (2002).
[64] P. W. Fowler, P. Lazeretti, and R. Zanasi, Chem. Phys. Lett. **165**, 79 (1990).
[65] D. J. Tozer and N. C. Handy, J. Chem. Phys. **109**, 10180 (1998).
[66] M. R. Pederson and A. A. Quong, Phys. Rev. B **46**, 13584 (1992).
[67] S. J. A. van Gisbergen, J. G. Snijders, and E. J. Baerends, Phys. Rev. Lett. **78**, 3097 (1997).
[68] J.-I. Iwata, K. Yabana, and G. F. Bertsch, J. Chem. Phys. **115**, 8773 (2001).
[69] R. Antoine, Ph. Dugourd, D. Rayane, E. Benichou, M. Broyer, F. Chandezon, and C. Guet, J. Chem. Phys. **110**, 9771 (1999).
[70] A. Ballard, K. Bonin, and J. Louderback, J. Chem. Phys. **113**, 5732 (2000).
[71] S. J. A. van Gisbergen, J. G. Snijders, and E. J. Baerends, J. Chem. Phys. **109**, 10644 (1998).
[72] S. J. A. van Gisbergen, J. G. Snijders, and E. J. Baerends, J. Chem. Phys. **109**, 10657 (1998).
[73] S. J. A. van Gisbergen, J. G. Snijders, and E. J. Baerends, Comput. Phys. Commun. **118**, 119 (1999).
[74] D. Jonsson, P. Norman, K. Ruud, H. Ågren, and T. Helgaker, J. Chem. Phys. **109**, 572 (1998).
[75] A. Warshel and M. Karplus, J. Am. Chem. Soc. **94**, 5612 (1974).
[76] Z. C. Wu, D. A. Jelski, and T. F. George, Chem. Phys. Lett. **137**, 291 (1987).
[77] S. J. Cyvin, E. Brendsdal, B. N. Cyvin, and J. Brunvoll, Chem. Phys. Lett. **143**, 377 (1988).
[78] D. E. Weeks and W. G. Harter, J. Chem. Phys. **90**, 4744 (1989).
[79] R. A. Jishi, R. M. Mirie, and M. S. Dresselhaus, Phys. Rev. B **45**, 13685 (1992).
[80] C. H. Choi, M. Kertesz, and L. Mihaly, J. Phys. Chem. A **104**, 102 (2000).
[81] P. Pulay, G. Fogarasi, G. Pongor, J. E. Boggs, and A. Vargha, J. Am. Chem. Soc. **105**, 7037 (1983).
[82] E. B. Wilson, J. C. Decius, and P. C. Cross, *Molecular Vibrations* (McGraw-Hill, New York, 1955).
[83] J. Onoe and K. Takeuchi, Phys. Rev. B **54**, 6167 (1996).
[84] R. Ditchfield, Mol. Phys. **27**, 789 (1974).
[85] A. K. Jameson and C. J. Jameson, Chem. Phys. Lett. **134**, 461 (1987).
[86] R. Taylor, J. P. Hare, A. K. Abdul-Sada, and H. W. Kroto, J. Chem. Soc. Chem. Commun. **1990**, 1423.
[87] S. G. Kukolich, J. Am. Chem. Soc. **97**, 5704 (1975).
[88] C. J. Jameson, A. K. Jameson, D. Oppusungu, S. Wille, and P. M. Burrell, J. Chem. Phys. **74**, 81 (1981).
[89] J. Gauss and J. F. Stanton, J. Chem. Phys. **103**, 3561 (1995).
[90] C. Joachim, J. K. Gimzewski, and A. Aviram, Nature (London) **408**, 541 (2000).